Atmospheric Research 304 (2024) 107382

Contents lists available at ScienceDirect

Atmospheric Research

journal homepage: www.elsevier.com/locate/atmosres

Improving the lightning forecast with the WRF model and lightning data assimilation: Results of a two-seasons numerical experiment over Italy

Stefano Federico [a], Rosa Claudia Torcasio [a,*], Jana Popova [b,c], Zbyněk Sokol [b], Lukáš Pop [b], Martina Lagasio [d], Barry H. Lynn [e,f], Silvia Puca [g], Stefano Dietrich [a]

[a] National Research Council of Italy—Institute of Atmospheric Sciences and Climate (CNR-ISAC), via del Fosso del Cavaliere 100, 00133 Rome, Italy
[b] Institute of Atmospheric Physics, Czech Academy of Sciences, Boční II 1401, 141 00 Prague, Czech Republic
[c] Faculty of Science, Charles University, Albertov 6, 128 00 Prague, Czech Republic
[d] CIMA Research Foundation, Via A. Magliotto 2, 17100 Savona, Italy
[e] Department of Earth Sciences, Hebrew University of Jerusalem, Givat Ram, Jerusalem 91904, Israel
[f] Weather It Is, Ltd., Efrat 91344, Israel
[g] Civil Protection Department, Via Vitorchiano 2, 00189 Rome, Italy

ARTICLE INFO

Keywords:
Lightning forecast
Lightning data assimilation
WRF
Convection
Forecast performance

ABSTRACT

We show, for the first time over Italy and over part of the central Mediterranean Basin, the impact of lightning data assimilation (LDA) on the strokes forecast for a long period. We use the Weather Research and Forecasting (WRF) model coupled with the Dynamic Lightning Scheme (DLS) at convection allowing horizontal resolution (3 km). We carried out a two-seasons experiment (summer 2020 and fall 2021) providing the forecast of lightning and precipitation for the next 6 h (nowcasting), considering two sub-periods (0-3 h and 3-6 h) for verification. The LDA is done through a nudging scheme that increases the water vapor mass in the mixed-phase region based on observed flash density rates and simulated graupel mixing ratio. No changes are made to the model run if spurious convection is predicted or no flashes are observed. LDA can trigger convection missed by the control forecast, without LDA, and/or can redistribute the strokes predicted to be more consistent with observations. LDA has a positive impact on strokes forecast, improving correct forecasts and reducing false alarms. This improvement is however confined to the first three-hours of forecast with negligible to negative impact for longer time ranges, in line with other studies. The improvement pattern is different in summer and fall, depending on the convection development.

The analysis of the Fraction Skill Score shows the usefulness of the forecast for practical purposes, considering the current areas used by the Civil Protection Department to issue meteorological alerts for intense convective events over Italy. Finally, it is shown that the forecast at the short-range ($0-3h$) using LDA can improve the strokes forecast issued on the previous day, not using LDA, and the methodology of this paper can be applied to issue warnings and alerts as the storm is approaching.

A brief examination of rainfall forecast shows positive impact of LDA at the short-range (0-3 h), with neutral impact for longer time ranges. The different impact of LDA on the strokes and precipitation forecasts is also highlighted.

1. Introduction

Lightning is a serious threat to life and properties (American Meteorological Society, 1924a, 1924b; Lopez and Heitkamp, 1995; Holle et al., 1996; Lopez and Holle, 1996; Rorig and Ferguson, 2002; Hodanish et al., 2004; Holle et al., 2005; Ashley and Gilson, 2009; Schultz et al., 2009; Wallmann et al., 2010; Koshak et al., 2015) and several humans activities such as aviation, recreation, electrical industries, outdoor activities, and others are influenced by it. There are many areas that are impacted by lightning around the world, both in the northern and southern hemisphere (Holle et al., 2018). The Mediterranean is among these areas and, as it is a populated area with frequent thunderstorms and lightning, the lightning forecast is of practical importance for public safety and economic activities.

* Corresponding author.
E-mail address: rc.torcasio@isac.cnr.it (R.C. Torcasio).

https://doi.org/10.1016/j.atmosres.2024.107382
Received 31 October 2023; Received in revised form 27 February 2024; Accepted 26 March 2024
Available online 31 March 2024

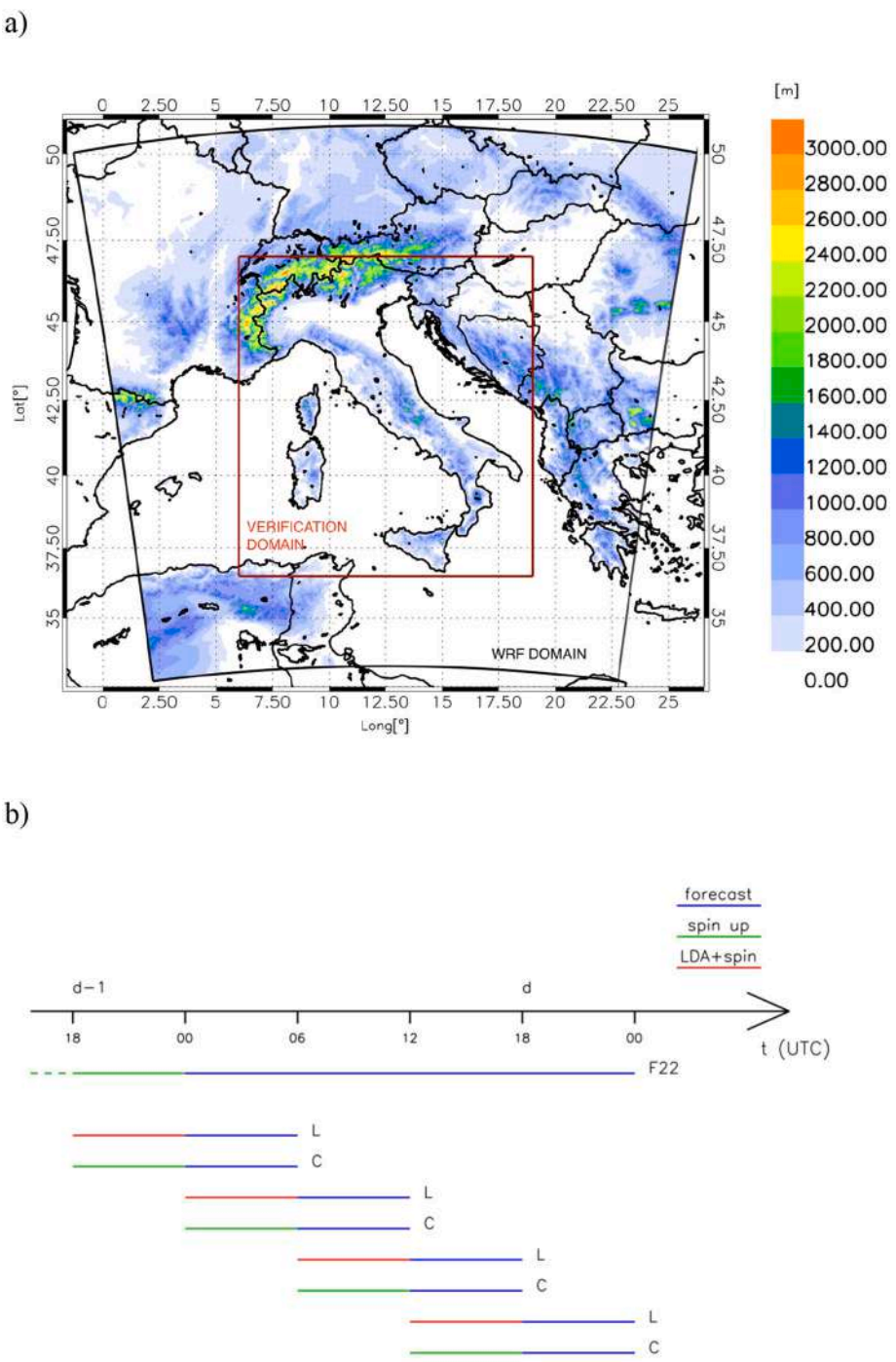

Fig. 1. a) the WRF domain with orography (colour scale [m]) and the verification area of strokes forecast (red square); b) the VSF configuration. L is the forecast using LDA, C is the forecast without LDA, F22 is the forecast issued on the previous day discussed in Federico et al. (2022).

There are two different approaches to forecast lightning. The first type contains methods that explicitly simulate the electric field in the clouds and its breakdown such as in Solomon and Baker (1996), Solomon et al. (2005), Mansell et al. (2002, 2005), Barthe et al. (2005, 2010), MacGorman et al. (2001), Popová et al. (2022, 2023). These methods can be one dimensional or three dimensional and Fierro et al. (2013) implemented a three-dimensional explicit method in the Weather Research and Forecasting (WRF) model (Skamarock et al., 2019). The explicit methods, however, are challenging in an operational context as they require a considerable amount of computing power.

The second type of methods forecast lightning indirectly via parametrization using the dynamic, thermodynamic and microphysical fields computed by a numerical weather prediction model (NWP) to predict lightning (Price and Rind, 1992; McCaul et al., 2009; Yoshida et al., 2009; Yair et al., 2010; Dahl et al., 2011; Wong et al., 2013; Federico et al., 2014; Lagasio et al., 2017; McCaul Jr. et al., 2020; Mittermaier et al., 2022). These methods need calibration before their operational use, nevertheless they are computationally efficient and can be useful for predicting the lightning threat. The methods using the microphysical fields outperform those based on thermodynamic fields only (Williams and Renno, 1993; Romps et al., 2018).

Lynn et al. (2012) introduced the Dynamic Lightning Scheme (DLS), which shares characteristics with the two approaches introduced above. It does not simulate explicitly the electric field, as in sophisticated

explicit lightning schemes, nor uses statistical relationship to compute the flash rate starting from dynamic, thermodynamic, and microphysical fields simulated by an NWP. Rather, it adds three prognostic equations to the WRF model to calculate the electrical potential energy for positive and negative cloud-to-ground and intracloud lightning. The electric energy can be advected by the model and the strokes are computed from these potentials. Former studies (Lynn et al., 2012; Lynn et al. (2015), Lynn (2017); Federico et al., 2022) applied the DLS with success, and the method is used also in this study.

As lightning is a manifestation of deep convection and can locate it precisely in space and time, it has been widely used to improve the forecast of severe and extreme weather events through lightning data assimilation (LDA). The techniques to assimilate lightning in NWP can be divided in two main groups, depending on the horizontal resolution of the NWP, i.e. if (i) it is used at scales that need convection parameterisation (>4 km) or (ii) it is used at convection allowing scales (4 km or finer; Lynn et al., 2020).

Considering the first group, lightning was assimilated based on relationship between lightning and other parameters that could be assimilated in NWP (Alexander et al., 1999; Chang et al., 2001; Jones and MacPherson, 1997; Papadopoulos et al., 2005; Pessi and Businger, 2009). Among them, Papadopoulos et al. (2005) used lightning to locate convection and then nudged the water vapor profile of the NWP towards profiles observed during convective events. Mansell et al. (2007) used lightning to trigger the Kain-Fritsch (Kain and Fritsch, 1990) cumulus scheme of the WRF also giving the advantage to suppress spurious convection when the model simulated unobserved lightning. This method was applied with success over Greece (Giannaros et al., 2016), where the precipitation forecast was improved up to 24 h for some cases.

Fierro et al. (2012) introduced LDA in a convection allowing NWP model (WRF) at 3 km horizontal resolution using a methodology that increases the water vapor mass in the mixed-phase region (0 °C/−20 °C layer) based on observed lightning flash density rates and simulated graupel mixing ratio. Other works followed (Fierro et al., 2014; Fierro et al., 2016) showing the positive impact of the LDA on the forecast of severe weather events and the comparison between LDA and radar data assimilation, which suggests a similar role of the two sources for the improvement of the forecast of intense convective weather events. The method was also adapted in other papers (Qie et al., 2014; Chen et al., 2019) to consider other hydrometeors and the dynamical field.

The scheme of Fierro et al. (2012) has been widely used over Italy to assess the impact of LDA on the precipitation forecast at the very short-range (3 h in most cases). Starting from the first work of Federico et al. (2017), who showed the potential of LDA to improve the precipitation forecast of deep convective events with the Regional Atmospheric Modeling System at Institute of Atmospheric Sciences and Climate (RAMS@ISAC) model, the methodology has been refined and used together with radar reflectivity data assimilation (Federico et al., 2019; Federico et al., 2021; these papers give also more details about the RAMS@ISAC model). Other experiments were performed with WRF (Comellas Prat et al., 2021; Torcasio et al., 2021) showing the significant and positive impact of LDA in the prediction of intense precipitation over Italy.

Lynn et al. (2015) and Lynn (2017) applied the LDA to improve the lightning prediction. Forecasts using and not using LDA produced economic savings over forecasts made with climatology, although not for all cost/loss ratios. In addition, the lightning assimilation scheme led to a faster and more accurate spin-up of initial convection and to the improvement of lightning forecast. However, for summertime storms, the advantage of using LDA was confined to the first three hours of forecast.

In a recent paper, Federico et al. (2022, hereafter F22) studied the performance of the DLS for strokes forecast over Italy for the next day using the WRF model. Their results showed that the lightning forecast upscaled to 24 km horizontal resolution can be used with success in the operational context of the Civil Protection Department of Italy (CPD). However, they did not use the LDA.

In this paper, we consider the possibility to improve the lightning forecast through LDA. As we are forecasting and assimilating convective environments, which are difficult to predict precisely at long time ranges, our focus is on the very short-term forecast (6 h). Two complete seasons are considered: Summer 2020 and Fall 2021, which have different characteristics and challenges for lightning forecasting over the Mediterranean area. As the summer 2020 superimposes with a period analysed in F22, a direct comparison of the results of this paper with those of F22 will be provided.

The paper is organized as follows: after this introductory Section 1, Section 2 shows the WRF model and the Very Short-term Forecast (VSF; 6 h). The DLS and the lightning data assimilation (LDA) methods are also presented in this section. Section 3 shows the results for strokes forecast, discussing the performance of LDA for two case studies, the statistics for the whole period, the spatial patterns of the forecast improvement, and the results for the fraction skill score. The results for the precipitation forecast and the comparison with the results of F22 are also discussed in this section. Finally, the discussion and conclusions are given in Section 4 and Section 5, respectively.

2. Data and methods

2.1. WRF model and experimental set-up

Simulations are done by the WRF model, version 4.1.3 (Skamarock et al., 2019). We use a grid with 3 km horizontal grid spacing and 635 × 635 grid points in the NS and WE directions. There are 50 vertical levels, with the model top at about 50 hPa. The model domain is shown in Fig. 1a. We used the following physical parameterizations: (Thompson et al., 2008) for the microphysics scheme, Mellor–Yamada–Janjic (Eta) for the boundary layer parameterisation (Janjic, 1994), Dudhia for the short-wave radiative scheme (Dudhia, 1989), and the rapid radiative transfer model (RRTM) for the longwave radiative scheme (Mlawer et al., 1997). Convection is assumed to be allowed at the horizontal resolution of this paper and no specific tests were done to assess the impact of parametrizing convection for this experiment. However, most of the papers using WRF at 3 km horizontal resolution do not use the convection parametrization (see for example Lynn et al., 2020), and our previous experience with this model over the same area (Torcasio et al., 2021; Comellas Prat et al. (2021)) suggest that the model has good performance in forecasting convection at 3 km horizontal resolution.

Initial and boundary conditions are taken from the European Centre for Medium range Weather Forecast (ECMWF) Integrated Forecasting System (IFS) operational analysis/forecast cycle at 0.25° horizontal resolution and issued at 12 UTC on the day before the actual day to forecast. Boundary conditions are updated every 3 h and the sea surface temperature is updated following the ECMWF-IFS analysis and forecast cycle.

We consider two kinds of experiments: a control simulation without lightning data assimilation, named C, and a lightning data assimilation experiment, named L. Both predictions follow a Very Short-term Forecast (VSF) approach, shown in Fig. 1b. Simulations are done over a 12 h period. For each simulation the first 6 h are used as spin-up time and for data assimilation for the L type. Forecast verification is then performed for the next 6 h of each run, considering two 3 h sub-periods: the first 3 h after assimilation (0-3 h) and the second 3 h after assimilation (3-6 h). Following this approach, 4 runs are needed to cover a whole day. Lightning is assimilated until 15 min before the starting forecasting time, i.e. 23:45 UTC for the 00–06 UTC forecast, 05:45 UTC for the 06–12 UTC forecast, 11:45 for the 12–18 UTC forecast, 17:45 for the 18–00 UTC forecast. This leaves 15 min to produce the forecast; using 256 cores of the ECMWF computing facility, we can forecast the first three hours of each period in < 15 min so that the forecast of the first 3 h is available just before its occurrence. It is important to note that this setting of the forecast is used in the agreement between the CPD and

CNR-ISAC and we are interested to verify this specific configuration.[1]

Results are also compared with the findings of F22, in which the strokes forecast issued on the previous day was considered. F22 simulations last 36 h, and the first 12 h are used as spin-up time. No data assimilation is performed in F22. In all cases the model output is saved every 3 h.

2.2. The lightning forecast

The method to forecast lightning is that of Lynn et al. (2012), and the reader is referred to this paper for the details about the scheme, while here we provide a brief description of it.

The scheme adds three equations to WRF computing the electric potentials of positive and negative cloud to ground strokes and of intracloud strokes. These potentials are calculated based on the Lightning Potential Index (LPI; Lynn and Yair, 2010; Yair et al., 2010), which quantifies the kinetic energy of the vertical motions scaled by the potential of charge separation. The latter is maximal when the graupel mixing ratio is present in equal ratio relative to liquid, ice and snow. The LPI is computed in the charging zone, between the freezing level and the isotherms −20 °C. The electric potential is given by the LPI multiplied by the total ice mass and divided by the charge of 1C.

As the cloud evolves, it builds up the electric energy, which is advected by the wind field. The source term for the electric energy per unit time is the power. It depends on the charge separated in the convective and stratiform clouds in one second. This current is a parameter of the scheme and is chosen to build up a reasonable amount of electric energy over a time interval. F22 applied the DLS to 162 cases over Italy and analysed the sensitivity of the scheme to the choice of the parameterised current, showing that the current of $0.75*10^{-4}$ A is the best setting among those tried. Thus, this current is used in this paper.

The discharge in the DLS is consistent with the tri-polar model of Williams (1989): negative strokes originate from the cloud base, positive strokes originate from the upper part of the cloud, while intra-cloud strokes originate everywhere within the cloud. The discharge occurs when/where the electric energy is larger than 10^9 J for negative cloud-to-ground (CG) and for intracloud (IC) strokes, and when/where electric energy is larger than $5*10^9$ J for positive strokes.

It is important to note that the 3 km resolution affects the prediction of small scale phenomena like strokes, which usually occur at the subgrid scale. In a previous study (Torcasio et al., 2023), it was shown that using the 2 km horizontal resolution increases the number of strokes simulated by the Lynn scheme compared to the 3 km horizontal resolution. However, it was also shown that a proper setting of the parameterised current in the scheme can be used to tune the number of simulated strokes to reach a reasonable agreement with observations.

The strokes forecast is verified by comparison with the LINET (LIghtning NETwork, Betz et al., 2004; Betz et al., 2009) observations. The network has > 200 sensors over Europe where it has the highest detection efficiency (DE). LINET sensors detect the low-frequency (LF) and very-low frequency (VLF) electromagnetic signals emitted by the flashes. The network can detect both CG and IC strokes but, in this paper, the attention is focused on the sum of IC and CG strokes. The position accuracy of the strokes is better than 100 m (Betz et al., 2009).

The LINET DE cannot be quantified over the investigated domain because we do not know the truth. Estimating the DE of a network as LINET is a difficult task and requires ad hoc experiments and/or Very High Frequency networks, which are not available. Also in these cases, however, the absolute DE can be difficult to estimate (Erdmann et al., 2020). The LINET DE is expected to be high over the investigated area because the LINET sensor measures the magnetic flux of the lightning signal directly as a function of time rather than the time derivative with subsequent integration (Betz et al., 2009). The relative DE of LINET compared to other networks was considered in several papers as Höller and Betz (2010) for the comparison with TRIMM-LIS, Lagouvardos et al. (2009) for the comparison with ZEUS network and in Defer et al. (2015) for some case studies of the HyMeX experiment (Ducrocq et al., 2014). In all cases the LINET performed very well. In these papers, however, the comparison referred to areas with partial or no overlap with the target area of this study. The ability of LINET to detect weak signals (<5 kA) over the target area is discussed in Petracca (2016).

2.3. The lightning data assimilation

For the LDA, we use the method of Fierro et al. (2012). Specifically, the water vapor mass mixing ratio simulated by the model is adjusted to the water vapor mixing ratio given by the following equation:

$$q_v = Aq_{vs} + Bq_{vs}tanh(CX)\left(1 - tanh\left(DQ_g^{\alpha}\right)\right) \quad (1)$$

where the coefficients are set to A = 0.95, B = 0.07, C=D = 0.25, and α = 2.2, and q_{vs} is the water vapor saturation mixing ratio, X is the gridded observed flash rate (units are number of flashes in the last 15 min), and Q_g is the simulated graupel mixing ratio (kg/kg). The adjustment is done in the mixed-phase region by direct substitution of the simulated water vapor, if the simulated graupel mixing ratio is <3 g/kg. Moreover, when the simulated water vapor mixing ratio is larger than the value of Eq. (1) its value is left unchanged. Hence, the water vapor adjustment consists in an increase of the air masses wet energy as a function of the gridded observed flash rate and of simulated graupel mixing ratio. The adjustment is applied to grid columns where flashes are observed ($X > 0$) by LINET, and no adjustment is applied where/when the model predicts spurious convection. For data assimilation, the observed flashes are gridded onto the 3 km WRF domain in 15 min time intervals during the first 5 h and 45 min of each simulation (therefore producing 23 periods for each 6 h assimilation window).

It is well known that the method of Fierro et al. (2012) can introduce a wet bias in the precipitation forecast and an attempt to reduce this bias was given in Lynn et al. (2015). In particular, they progressively nudged the hydrometeor mass values to zero wherever the model predicted spurious convection. However, the results on the strokes forecast were contrasting and further research is needed to apply this method. Recently, Erdmann et al. (2023) proposed a method to suppress spurious convection through LDA. In their approach, the simulated and observed Flash Extent Density (FED) is used to calculate a pseudo-profile of relative humidity (RH) that can increase (reduce) the modeled relative humidity if flashes are not simulated (simulated) but observed (not observed). However, this method is not available in WRF.

It is finally noted that, even if the method of Fierro et al. (2012) cannot suppress spurious convection, the data assimilation is a complex process that does not affect a single model variable but the forecast of the model trajectory in the phase space entirely. This can reduce the spurious convection forecast by the control simulation, not using LDA, in some cases. Examples of this behavior are given in Torcasio et al. (2021) and will be further discussed in this paper.

Strokes are grouped into flashes before data assimilation following Höller and Betz (2010), grouping into the same flash strokes within 1 s and within 10 km, but verification is done at the strokes level as the DLS predicts strokes. The average number of strokes grouped in the same flash is between 3 and 4 but there is a considerable variability. The flash location is determined by the average of the longitudes and latitudes of the strokes composing the flash, and lightning is assimilated as a point (we neglect its spatial estension). The grouping could introduce a spatial error in the flash position that, in the worst case, is $10\sqrt{2}$ km.

[1] The official model used by CPD to issue meteorological alerts over Italy is COSMO-ICON. WRF is applied by CNR-ISAC in collaboration with CPD to test specific aspects, as the assimilation of lightning data for the forecast of severe weather and convective events.

Table 1
Total elements of the contingency tables for precipitation and strokes.

	SUMMER 2020		FALL 2021	
	0-3 h	3-6 h	0-3 h	3-6 h
Precipitation	1,202,103 (62,354; 12,008; 1532)	1,206,290 (57,731; 10,503; 1371)	1,335,709 (114,821; 23,023;1794)	1,063,613 (91,560; 13,287;1550)
Strokes	756,240 (23,179; 14,136; 10,728)	756,240 (23,051; 14,022; 10,536)	748,020 (27,128; 13,292; 8210)	748,020 (27,495; 13,405; 8287)

The number in parentheses in the first row represent the number of observed events for the thresholds of 1 mm/3 h, 10 mm/3 h and 30 mm/3 h, which are considered in detail in Section 3.6. The number in parentheses in the second row represent the number of observed events for the thresholds of 1 stroke/(24km^2*3 h), 10 strokes/(24km^2*3 h) and 30 strokes/(24km^2*3 h), which are considered in detail in Section 3.2.

2.4. Performance verification

Model performance is verified both for lightning and precipitation forecasts against measurements. Observed strokes come from LINET (Section 2.2), while precipitation measurements are from the Italian raingauge network, which has about 4000 rain gauges over Italy. These data are managed by the Italian regional administrations and are collected nationwide at the CPD.

For the computation of scores, observed strokes are first remapped onto the WRF grid, then the observed and predicted strokes are upscaled from 3 km to 24 km, summing over 8 grid cells in both horizontal directions. Verification is therefore performed on a 24 × 24 km^2 cell, as in F22, to neglect in some measure spatial errors of strokes forecast. It is important to recall, however, that the area of 24 × 24 km^2 is smaller than the areas used by the CPD to issue meteorological alerts over Italy and this choice is compatible with the actual framework used by CPD. In addition, strokes observations are available over the area from 6° to 19° E and from 36.5° to 47° N, which is the verification domain (Fig. 1a). Lightning is accumulated over a 3 h period and verification is performed for the first three hours and for the next three hours after the end of the spin-up or spin-up+assimilation time (Fig. 1b).

For precipitation verification, we used the following method: we consider all model grid points in a radius of $2\sqrt{(}2)\Delta x$ from the raingauge, Δx being the model horizontal grid spacing (3 km in our case), and we select, among these points, the one whose value best matches the observation. This choice neglects model spatial errors of about 8.5 km, which mitigates the problem of the double-penalty error for very localized convective events. The method was widely used in previous papers over the same area (Federico et al., 2019; Comellas Prat et al., 2021), making the results of this paper comparable with these studies. It is important to highlight that, even though gauges provide a physically direct measure of precipitation and are here considered as the "truth", they have also errors. The main source of error is the under-catch, primarily caused by the wind effects around the gauge orifice (Peterson et al., 1998).

For strokes and precipitation, we compute the following scores: Frequency Bias (FBIAS), Probability of Detection (POD), Threat Score (TS), Equitable Threat Score (ETS), and False Alarm Rate (FAR). These scores are computed using 2 × 2 contingency tables for dichotomous events (that can assume one of the two values between "yes" and "no") for different thresholds. For each threshold the following event is considered: "is the precipitation or the number of strokes above that threshold?". The hits (a), false alarms (b), misses (c), and correct negatives (d) of the contingency tables are then computed for these events and the scores are defined as:

$$FBIAS = \frac{a+b}{a+c}$$

$$POD = \frac{a}{a+c}$$

$$TS = \frac{a}{a+b+c}$$

$$ETS = \frac{a-a_r}{a+b+c-a_r}$$

$$a_r = \frac{(a+b)(a+c)}{a+b+c+d}$$

$$FAR = \frac{b}{a+b}$$

where a_r is the expected number of correct forecasts above the threshold in a random forecast where forecast occurrence/non-occurrence is independent of observation/non-observation. The FBIAS has its best value at 1 and varies from 0 to $+\infty$. The POD and TS consider values in the interval between 0 and 1, and 1 is their perfect score. Also FAR varies in the interval between 0 and 1, but the perfect score is 0. ETS varies between $-1/3$ and 1, the latter value being the perfect score.

It is important to quantify the total size of the contingency tables ($N = a + b + c + d$) for strokes and precipitation to have an idea about the statistical robustness. This information is given in Table 1. In addition, we provide the number of observed events ($a + c$) for the strokes and rainfall thresholds considered in detail in Sections 3.2 and 3.6, respectively.

The FBIAS, POD, FAR, and TS scores are shown through a performance diagram (Roebber, 2009). In this diagram, the x-axis represents the Success Ratio (SR), which is defined as 1-FAR, while the y-axis represents the POD. The straight lines starting from the origin are constant value of FBIAS, and the hyperbole branches represent constant values of TS.

The statistical significance of the difference in the scores between control simulation without LDA (C) and forecasts assimilating lightning (L) is assessed by the resampling test proposed by Hamill (1999). Another method used to assess if a prediction is skillful is the Fraction Skill Score (Roberts and Lean, 2008; FSS). It is a neighborhood-based metric, which considers the square root error of the forecast relative to a worst reference forecast. The forecast is considered skillful if the FSS is larger than $0.5 + f_0/2$, where f_0 is the probability of occurrence of the event, which is < 2% for the stroke's occurrence over the area of interest and for the two seasons analysed in this paper. Lynn (2017), using a cost loss ratio analysis to evaluate the economic value of the total lightning forecast, showed that saving over climatology (SOC) can be attained for FSS values lower than 0.5, however the SOC increases for higher FSS. From those results, we consider the FSS > 0.5 as skillful for total lightning forecast. The computation of the FSS for the lightning forecast is detailed in F22.

3. Results

3.1. Two case studies

In this section we consider two examples of strokes prediction to show how the LDA can impact the forecast. In the first case, the control forecast missed the convection, while in the second case the area of convection was underestimated by the control forecast and a false alarm was predicted in northwestern Alps.

The first case study occurred on 25 August 2020 between 00 and 03 UTC (Fig. 2). At this time > 42,000 strokes were observed over the Balkans (Fig. 2a). The control forecast (Fig. 2b) missed the prediction of this convection with an unsatisfactory forecast of 4575 strokes. The

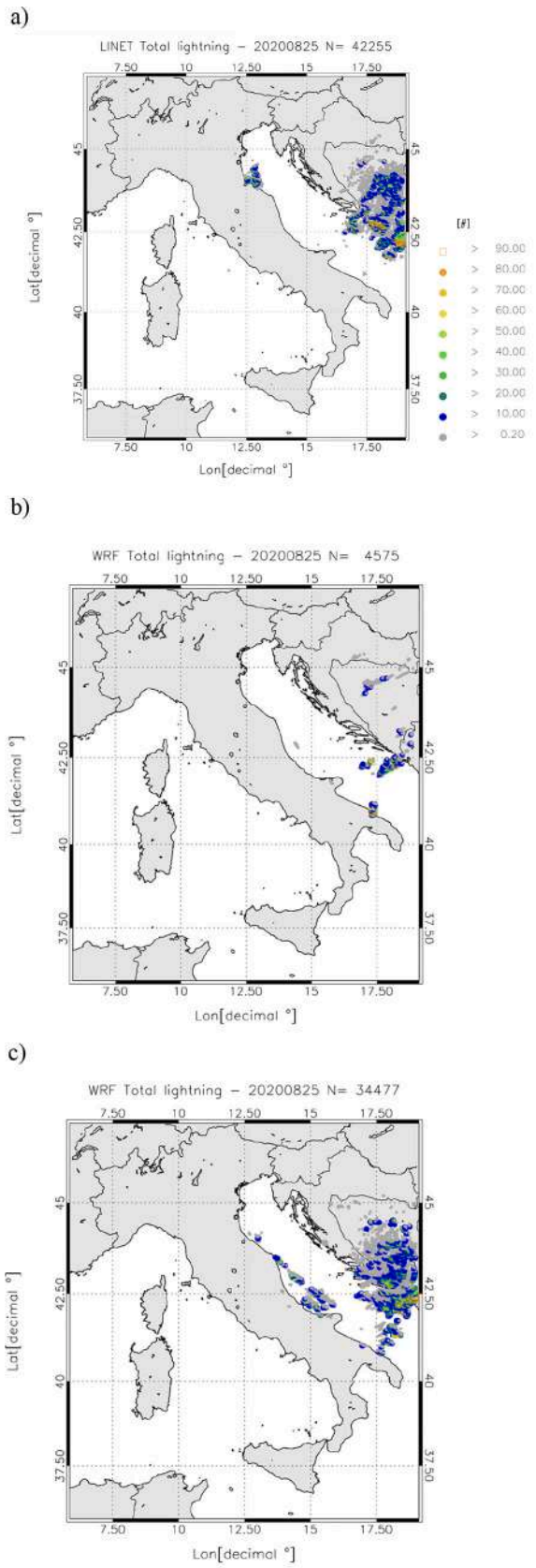

Fig. 2. Strokes between 00 and 03 UTC on 25 August 2020: a) observations by LINET; b) control forecast C; c) forecast L with LDA.

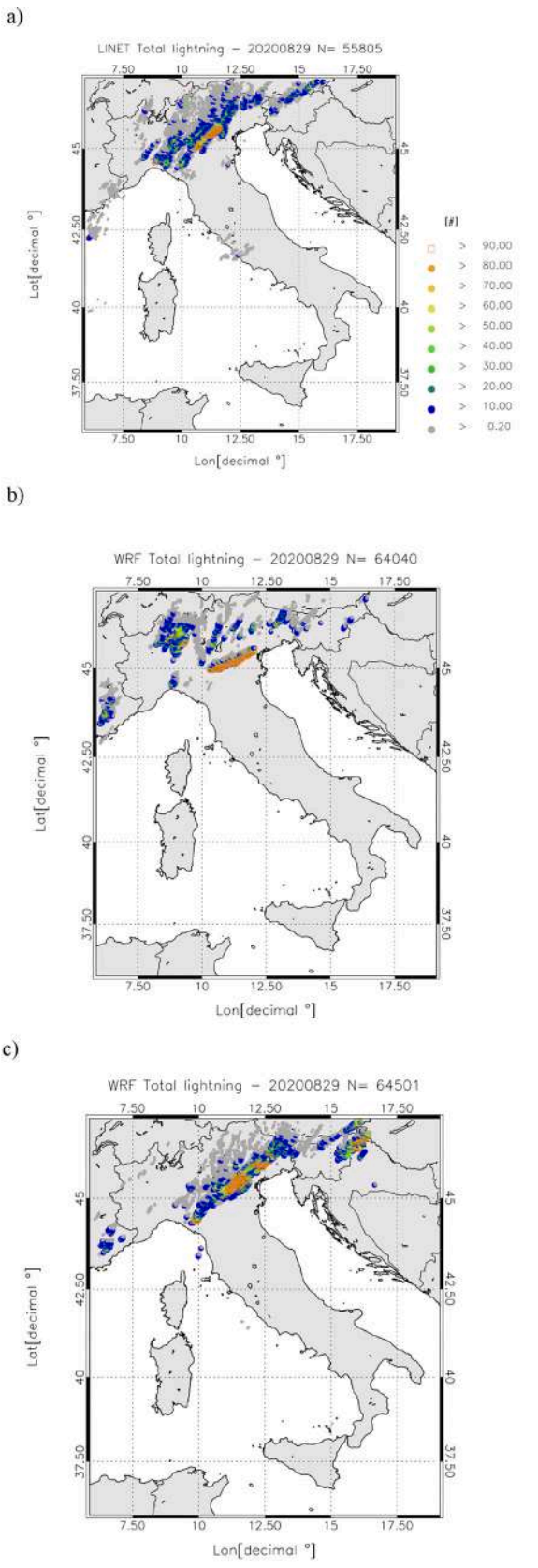

Fig. 3. Strokes between 12 and 15 UTC on 29 August 2020: a) observed by LINET; b) control forecast (C); c) forecast with LDA (L).

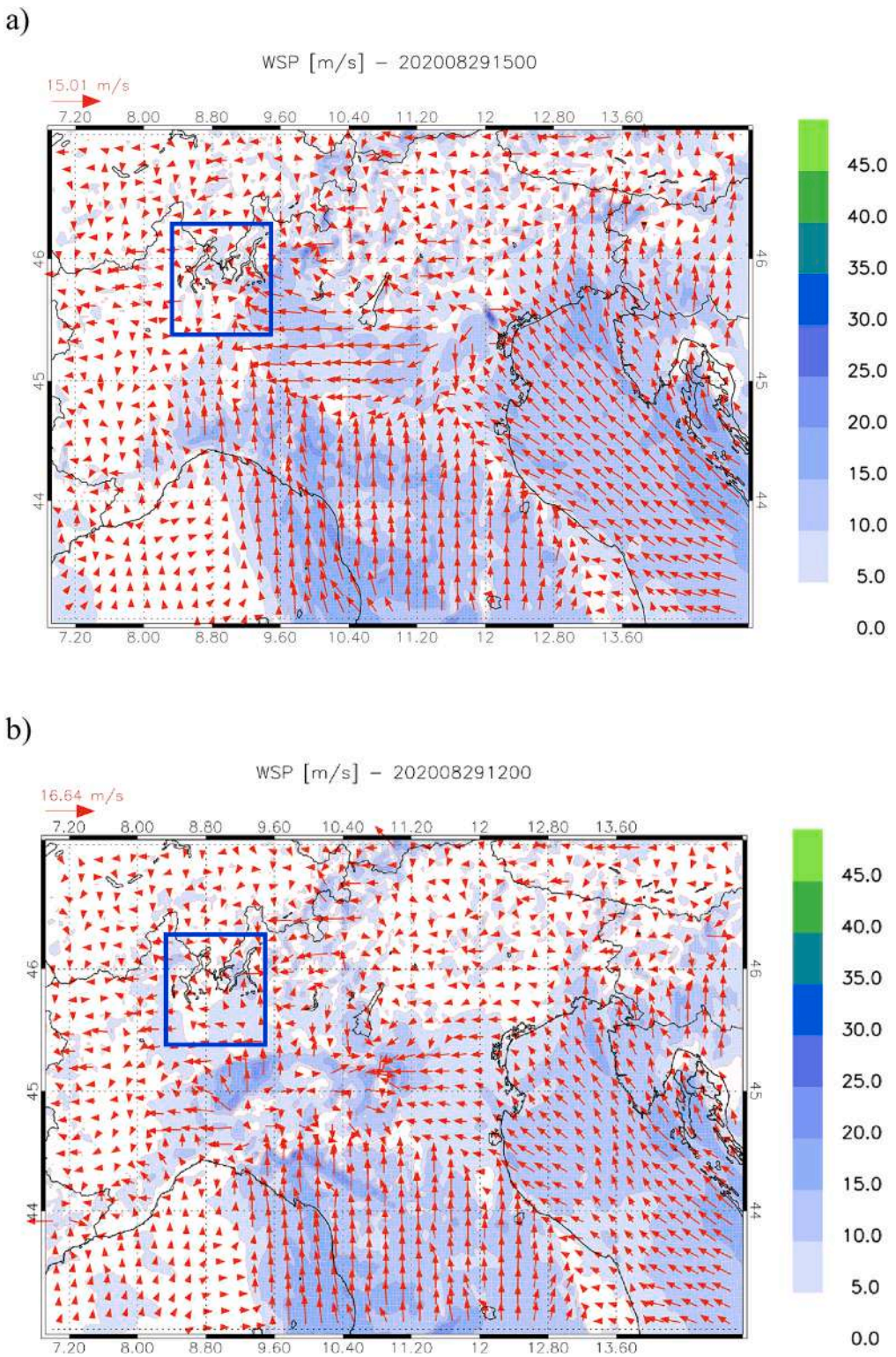

Fig. 4. a) winds at (about) 110 m above the surface for the control forecast at 12 UTC on 29 August 2020; b) as in a) for the forecast using lightning data assimilation. The blue box identifies the area of spurious convection referred into the text.

prediction of the simulation with LDA is much better as strokes are correctly forecasted over the Balkans. The number of strokes is slightly underestimated (34,474) compared to the observations and there are false alarms over the Adriatic Sea, however, the strokes forecast is much improved by LDA. The results of this specific case show that LDA can trigger the convection missed by the control forecast.

The second case study refers to an episode of convection which developed over northern Italy on 29 August 2020 between 12 and 15 UTC. In this case the number of observed strokes was 55,805 (Fig. 3a). The control forecast predicted convection over northern Italy (64,040 strokes; Fig. 3b) but the convection was more scattered compared to observations. In addition, the strokes over the northwestern part of the domain at about (8.75°E, 47°N) were false alarms.

The forecast of the strokes using LDA for this case (Fig. 3c) shows a

much better agreement with observations: the false alarms in the NW of Italy are not simulated and the convection is more extended than in the case of the control run. The number of lightning forecast by the simulations with or without data assimilation are similar (about 64,000), and, in this case, LDA redistributes the strokes more than adding new ones. However, there are false alarms simulated between Croatia and Slovenia, especially in the simulation with LDA.

As shown above, even if LDA adds moist static energy to the atmosphere, sometimes it can reduce the false alarms, as over Northwestern Alps for the second case study (29 August 2020). To analyze more in detail this point, we show in Fig. 4 the horizontal wind speed at the third WRF vertical level (about 110 m above the surface) over Northern Italy at 12 UTC for the control simulation and for the simulation with LDA. The control simulation shows a flow from East to West over Pianura

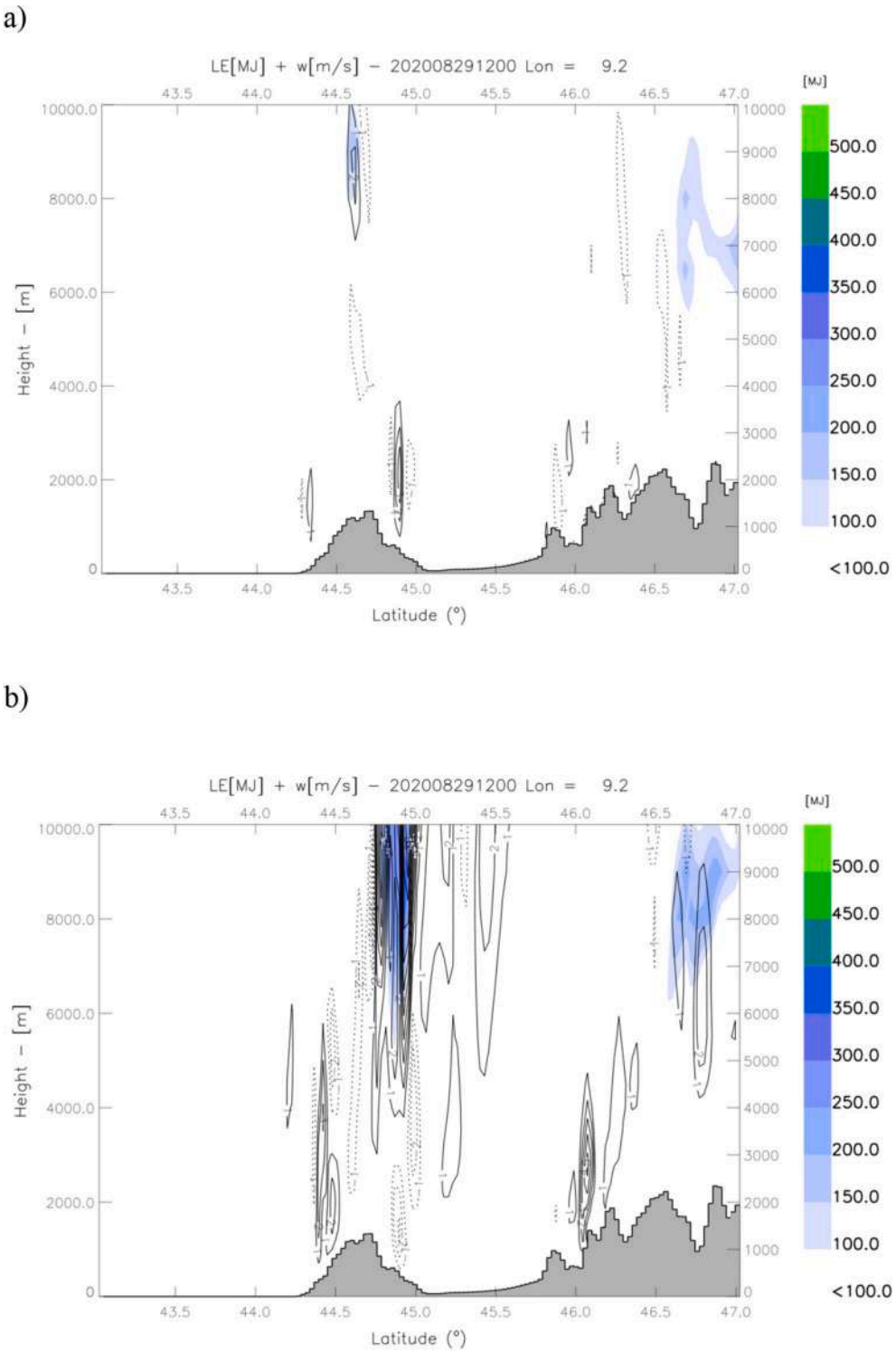

Fig. 5. a) latitude-height cross section at longitude 9.2°E for vertical velocity (contours from −10 m/s to 10 m/s every 1 m/s, the zero contour is not plotted) and electric energy (MJ; shaded contours) for the control forecast at 12 UTC on 29 August 2020; b) as in a) for the forecast with LDA; c) as in a) at 15 UTC; d) as in b) at 15 UTC.

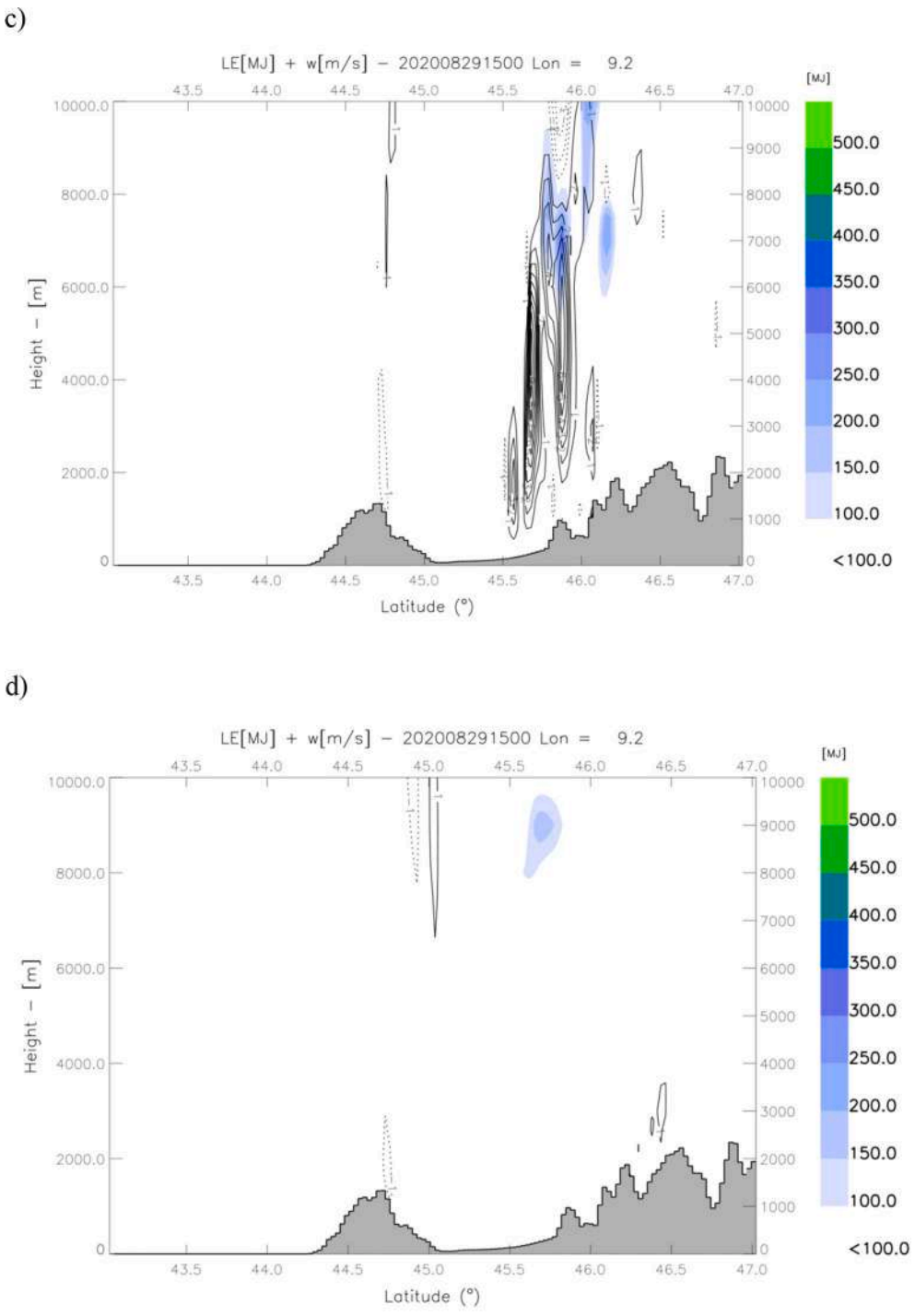

Fig. 5. (*continued*).

Padana bringing humid marine air-masses towards the Alps, including Northwestern Alps, where the convection was simulated by the control forecast (Fig. 3a; see also the blue box in Fig. 4). Horizontal winds are different in the simulation with LDA. There is a big thunderstorm developing in the southern flank of Pianura Padana that reduces, substantially, the advection of marine air-masses towards the Northwestern Alps, contrasting the convection development in this area. It is worth noticing that a similar consideration can be drawn for low and middle troposphere heights (up to 7000 m) and LDA changes substantially the evolution of the forecast.

This analysis is further confirmed by the cross sections of Fig. 5, showing the electric energy (see Lynn et al. (2012) for the computation of this parameter) and the vertical velocity at 12 and 15 UTC for the control forecast (panels a,c) and for the forecast with LDA (panels b,d). At 12 UTC the convection is only marginally developed in the control forecast, while it is well developed over the southern flank of Pianura Padana (around 45°N) in the simulation using LDA. Here, vertical velocities of updrafts and downdrafts are larger than 10 m/s and the electric energy reaches 350 MJ.

In the following hours, the combined effect of surface warming, of the valley-mountain flow and of the advection of humid air-masses, causes the development of deep convection over the Alps in the control simulation (Fig. 5c). This is apparent at 15 UTC, when vertical velocities up to 10 m/s develop and the electric energy reaches 350 MJ. On

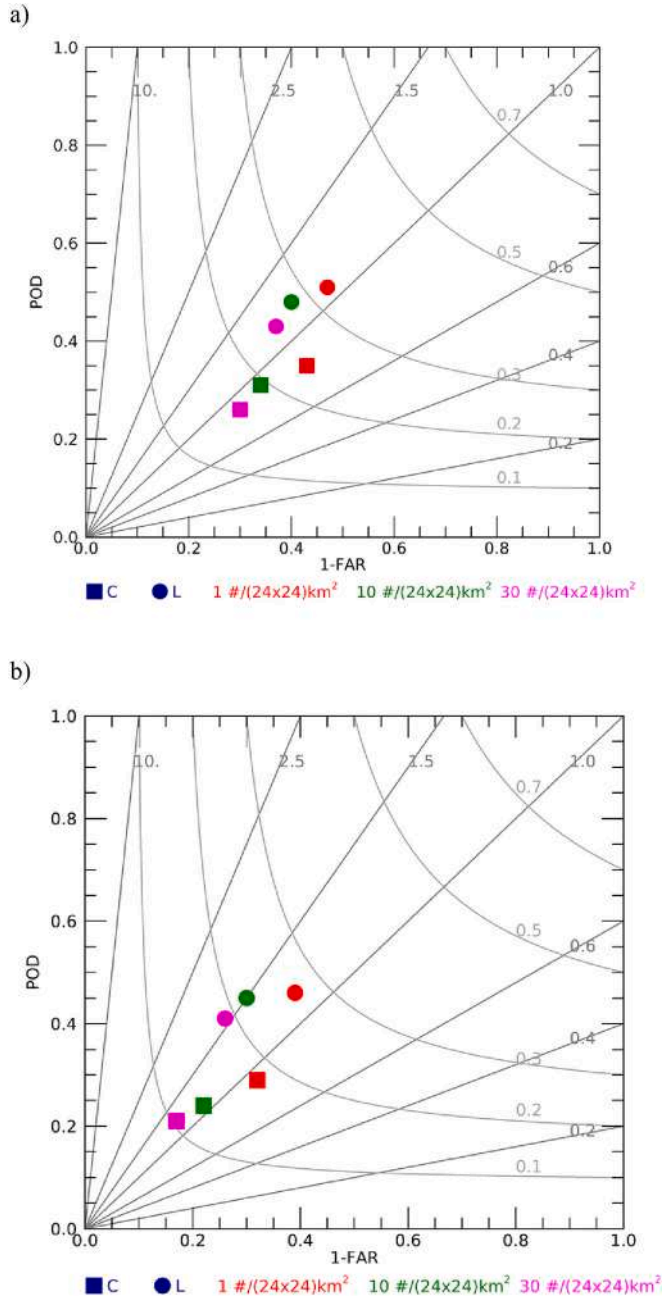

Fig. 6. Performance diagram for the first three forecast hours of strokes prediction for the experiments with (L, represented by filled circles) and without (C, represented by filled squares) LDA for summer (panel a) and fall (panel b). Red is for the 1 stroke/(24 km*24 km) threshold, green is for 10 stroke/(24 km*24 km), and magenta is for 30 stroke/(24 km*24 km). Straight lines represent constant values of FBIAS, while hyperbolic lines represent constant values of TS. (For interpretation of the references to colour in this figure legend, the reader is referred to the web version of this article.)

the contrary, the forecast with LDA does not predict the development of convection at 15 UTC (Fig. 5d). In summary, the situation at 12 UTC shows a well-developed convection over the southern flank of Pianura Padana forced by LDA and a much less intense convection developing in the control forecast, while the situation is reversed at 15 UTC (consistent profiles of relative humidity and temperature are simulated, not shown). Lightning observations show convective activity in the southern flank of Pianura Padana at 12 UTC with much less activity at 15 UTC and are in better agreement with the forecast using LDA compared to the control forecast. These results suggest that the LDA triggers the convection and

Table 2
Results of the statistical test for the difference between the score of simulations with and without LDA for summer 2020.

	Threshold (number of strokes/(24 km*24 km*3 h))						
	1	5	10	15	20	25	30
FBIAS	99;*95*	99;*99*	99;*99*	*99*;*99*	*99*;*99*	*99*;*99*	99;*99*
ETS	99;/	99;/	99;/	99;/	99;/	99;/	99;/
POD	99;/	99;/	99;/	99;/	99;/	99;/	99;/
FAR	99;90	99;90	99;90	99;90	99;90	99;90	99;90

The numbers indicate the significance level (90, 95 or 99). Plain text values show a positive impact of LDA on the scores (i.e. the value of the score for simulations with LDA is closer to the perfect value compared to the control forecast), values in italic indicate a negative impact of LDA on the scores (i.e. the value of the score for control simulations is closer to the perfect value compared to the forecast with LDA). The first number in each cell is for the 0-3 h forecast phase, the second number is the score for the 3-6 h phase. Results are shown for thresholds from 1 to 30 strokes per grid cell (24*24 km^2) per 3 h.

Table 3
As in Table 2 but for fall 2021.

	Threshold (number of strokes/(24 km*24 km*3 h))						
	1	5	10	15	20	25	30
FBIAS	*99*; *99*	*99*; *99*	*99*; *99*	*99*; *99*	*99*; *99*	*99*; *99*	*99*; *99*
ETS	99; /	99; /	99; /	99; /	99; /	99; /	99; /
POD	99; *99*	99; *99*	99; *99*	99; *99*	99; *99*	99; *99*	99; *99*
FAR	99; 99	99; 99	99; 99	99; 99	99; 99	99; 99	99; 99

For fall we found either 99% or no significance.

can change substantially the evolution of the forecast. On some occasions, this can suppress spurious convection predicted by the control forecast.

These results show an improvement of the strokes forecast using LDA. This improvement can be new convection forced by LDA that is missed by the control forecast, or a better representation of the convection partially simulated by the control forecast.

While for most cases we found an improvement of the strokes forecast by LDA, there are occasions when LDA does not improve or has a negative impact on the strokes forecast. Two main types of events were found looking at the model output: a) cases when there are very few or no flash assimilated (< 100 flashes; in cases of no flashes assimilated the control forecast and the forecast with LDA give the same results); b) cases where there is (mostly weak) scattered convection over the domain. The point a) is obvious. As regards point b), in cases of scattered convection, it may occur that flashes are assimilated in places far from the strokes observed in the following hours. In these cases, WRF can simulate convection in places close to positions where flashes are assimilated but, in these places, flashes are not observed in the following hours, giving false alarms.

3.2. Strokes forecast for the whole domain and for the two seasons

After showing examples of the impact of LDA on the strokes forecast for specific cases, it is important to have a statistically robust quantification of LDA performance for the whole domain and the whole period. We consider the statistics for summer 2020 and fall 2021 and for the first three hours (interval 0-3 h after the end of the spin-up/assimilation phase) and for the second three hours (interval 3-6 h after the end of the spin-up/assimilation phase) of forecast.

Results for summer 2020 and fall 2021 are represented by the performance diagram in Fig. 6 for three different strokes intensities (1, 10 and 30 strokes per 24*24km^2 grid cell) and for the first three hours of forecast. The performance diagrams show a substantial improvement of the strokes forecast when LDA is used: the L forecast is always closer to the upper right corner compared to the C forecast. The performance

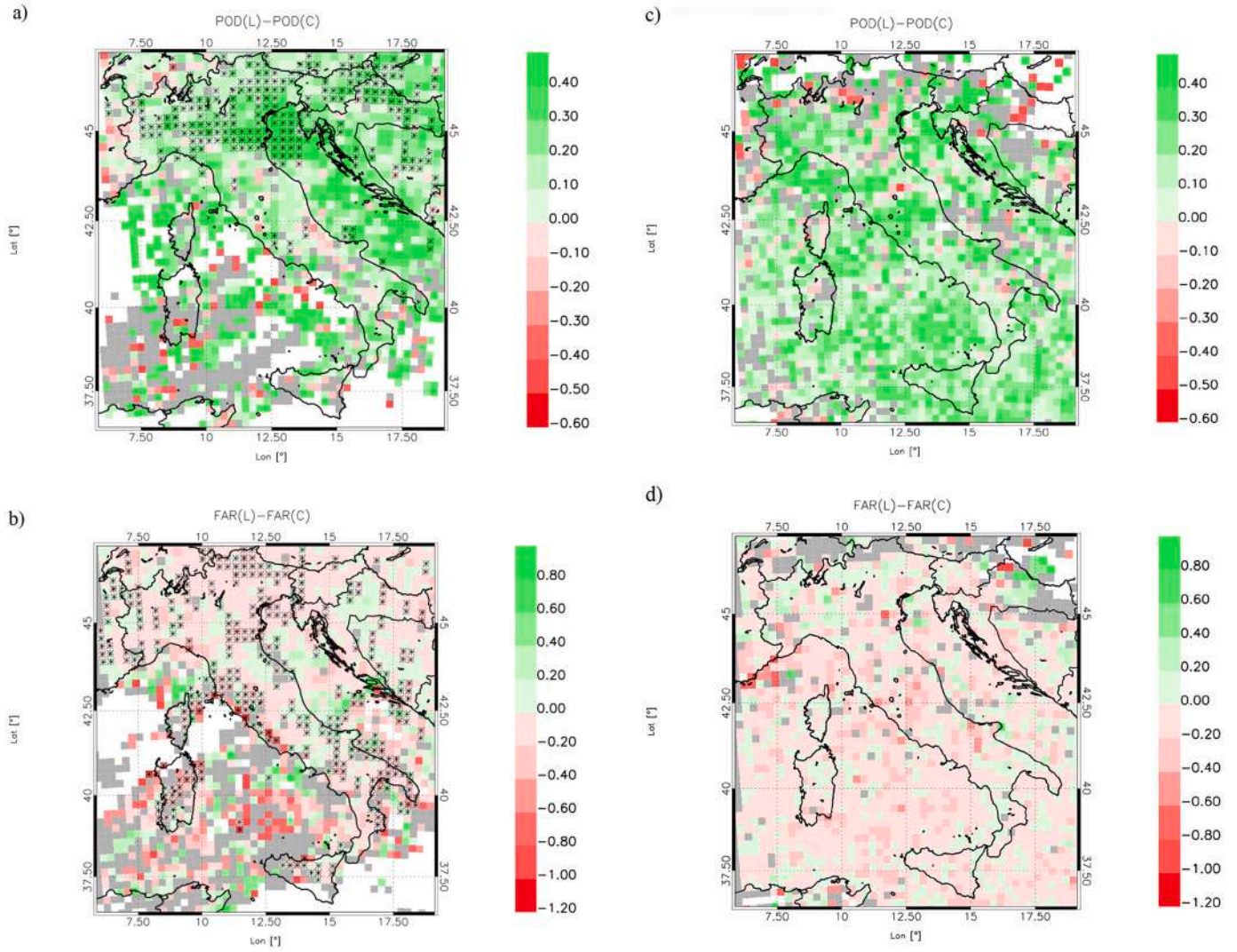

Fig. 7. Difference of the scores between the forecast with LDA and the control forecast (in this order): a) POD for summer 2020; b) FAR for summer 2020; c) POD for fall 2021; d) FAR for fall 2021. Greenish colors are positive values, reddish colors are negative values. Grey colors represent grid cells with the same score values for C and L. The differences are computed for all simulations in each season, considering the first 3 h of forecast and the threshold of 1 stroke per grid cell (24*24 km^2) per 3 h. Asterisks show grid cells where the statistical significance of the difference of the scores is larger than 90%.

decreases with increasing thresholds, showing the difficulty of the model to forecast precisely the most intense convection. It is also noted that, as expected by the method used to assimilate lightning, the FBIAS of the simulations with LDA increases compared to the control simulations. This is especially apparent in fall (Fig. 6b), where the LDA has a negative impact on the FBIAS. Summer scores (Fig. 6a) outperform the corresponding values in fall both for C and L. This result is confirmed by further analyses discussed later.

Results for the 3-6 h phase (not shown) reveal a small to negligible impact of LDA on the strokes prediction and, for the experiment considered in this work, LDA improves the lightning forecast at the short-range (0-3 h) only.

Statistical significance of the difference of the scores for the experiments with and without data assimilation using the resampling method of Hamill (1999) is shown in Tables 2 and 3 for summer and fall, respectively. Considering the results for summer, we note a significant improvement of the forecast for the first three hours of forecast, with some exceptions for the FBIAS. Interestingly, both the POD and the FAR are improved. The improvement of both the hits and the false alarms has a significant and positive impact on the ETS score. For the second three hours of forecast, the LDA has a negligible impact on the strokes forecast; the FAR is improved while FBIAS is worsened. The inspection of the model output reveals that the FBIAS of the phase 3-6 h of the forecast with LDA (not shown) is lower than 1 and lower than that of the control forecast. This behavior is likely related to the (excessive) amount of moist static energy added to model through LDA, which could have left too stable atmospheric conditions after the first three hours of forecast. However, other issues as the simple nudging scheme to assimilate lightning could have played a role, and studies are currently in progress to better understand if using the 3DVar to assimilate lightning can improve this issue.

Results for fall show again a positive impact of LDA on both POD and FAR for the first three hours of forecast (Table 3). As POD and FAR are improved, the ETS score has a notable improvement for all thresholds. The LDA tends to increase the number of predicted strokes as shown by the FBIAS score, which is significantly worse in the forecast with LDA compared to the control forecast and shows an overestimation of the frequency of the events (Fig. 6b), even if better colocated with observations. The positive impact of LDA is limited because the method doesn't suppress explicitly the spurious convection, as for example in Erdmann et al. (2023) or Lai et al. (2019).

During the forecast phase 3-6 h there is a negative impact of LDA on

Table 4
First column: score; Second column: number of grid cells where the scores are improved by LDA over the domain of Fig. 7; third column: number of grid cells where LDA has a negative impact on the score; fourth column: percentage of improved grid cells computed respect to the total number of grid cells of Fig. 7 (2055); fifth column: percentage of grid cells with negative impact of LDA on the strokes forecast computed respect to the total number of grid cells (2055).

SCORE	Improved	Worsened	Percentage improved	Percentage worsened
FBIAS	1051	821	52	40
ETS	1312	576	64	28
POD	1399	173	68	8
FAR	906	512	44	24

Statistics refer to summer, to the 1 stroke in 3 h per grid cell (24*24 km^2) threshold, and to the first three hours of forecast.

Table 5
As in Table 4 for fall.

SCORE	Improved	Worsened	Percentage improved	Percentage worsened
FBIAS	969	1073	47	52
ETS	1538	451	75	22
POD	1617	167	79	8
FAR	1317	518	64	25

the strokes forecast, as shown by the significant decrease of the POD for all thresholds. Considerations similar to summer apply, and further studies are required to improve this issue.

The results of this section show that the lightning forecast is substantially improved by LDA for the first three hours of forecast, while there is small to negative impact for the following three hours.

3.3. *Patterns for summer and fall improvements*

It is interesting to show the spatial patterns of the improvement of lightning forecast for the two seasons during the first three hours of forecast to understand the results in more detail. Fig. 7 shows the difference of the POD (panels a and c) and FAR (panels b and d) for summer (panels a and b) and fall (panels c and d) between the strokes forecast with LDA and the control forecast. The threshold considered is 1 stroke per 3 h per 24*24 km^2. A positive difference in POD means that the simulation with LDA has a higher POD compared to the control forecast; conversely a negative difference of the POD score means that the forecasts with LDA performs worse than the control forecast. There are grid cells where the POD of the control and that of the simulations assimilating lightning could not be computed (no observations of lightning for this grid cell for the period), which are represented by white cells. There are cases when the POD score of the control forecast and that of the forecast with LDA have the same value and they are represented as grey grid cells.

The POD for summer is improved by LDA as shown by the larger amount of green grid cells compared to red grid cells in Fig. 7a. In particular, the improvement is more apparent over the Italian mainland, over the Balkans and over the Adriatic Sea. The FAR improvement is given by the reddish grid cells of Fig. 7b; in this case the largest improvement is over the Tyrrhenian Sea and the Italian west coast. The appearance of Fig. 7a and b is confirmed by the results of Table 4, which shows the number of grid cells and the percentages of the total grid cells improved by LDA and extends the analysis to FBIAS and ETS. The ETS is improved in 1312 grid cells (64%) and it is worsened in 576 grid cells (28%). The pattern of the improvement (not shown) is similar to that of POD (Fig. 7a). FBIAS is also improved for this specific threshold (1051 grid cells are improved, while the score is worsened in 821 grid cells), however the impact is much lower compared to other scores.

As shown in the previous section, the L and C strokes forecasts are statistically different considering the whole domain, at least for the first

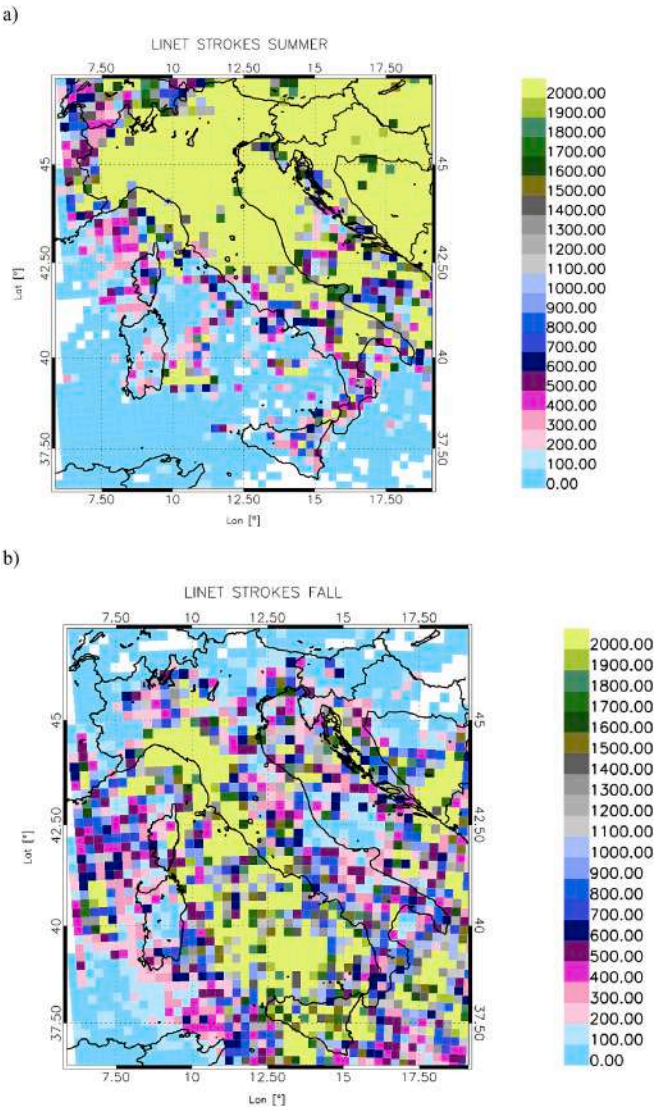

Fig. 8. Total number of lightning assimilated in WRF in summer (panel a) and in fall (panel b). White cells represent cases with zero lightning recorded.

3 h of forecast. The statistical difference was also evaluated for each grid cell at 90% level for the 1 stroke per grid cell (24*24 km^2) per 3 h threshold. Grid cells where L and C difference is statistically significant are indicated by the asterisks in Fig. 7 (note that no grid cells were found in fall). Attaining the statistical significance for grid cells is very difficult for two main reasons: a) the number of events is drastically reduced compared to the number of events for the whole domain; b) if a storm occurs over a portion of the domain (the most common situation), the impact of LDA is mainly in the portion of the domain interested by the storm with some effect downstream, while for other grid points the situation is unchanged. As a consequence, a much longer period must be considered to attain the statistical significance for individual grid cells.

Fig. 7c shows the POD difference between the simulation with LDA and the control forecast in fall 2021, while statistics are reported in Table 5. The grid cells where the forecast is improved (1617, i.e. 79% of the total grids cells) are mainly located over the Italian mainland and over the Tyrrhenian Sea. Interestingly, this pattern is complementary to that of summer. If we divide the domain of Fig. 7 in two parts with a diagonal connecting the NW corner to the SE corner, the improvement in summer is mainly in the northeastern half of the domain, while the improvement in fall is mainly in the southwestern half of the domain. The FAR, Fig. 7d, is improved by LDA in 1317 grid cells (64% of the grid

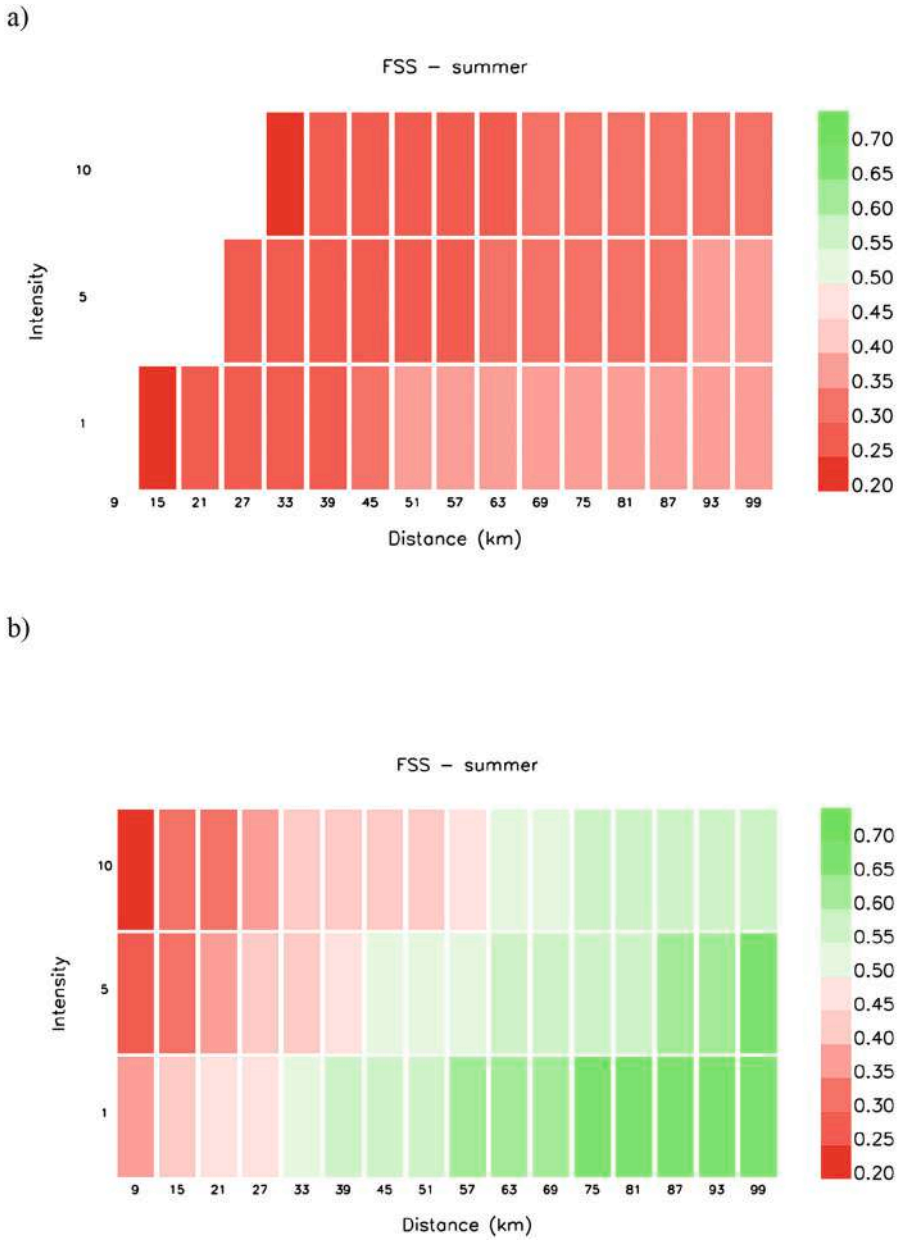

Fig. 9. FSS for summer 2020 for different length scales (*x*-axis from 9 to 99 km) and for different intensities of the strokes (1, 5, 10 strokes per grid cell of the WRF model): a) control forecast (C); b) forecast with LDA (L). Greenish colors show skillful forecasts. White cells are values below 0.2.

cells), while it worsened in 518 grid cells (25%). However, for this score, the pattern of the improvement is rather uniform over the domain. The ETS score is clearly improved in fall (Table 5), while it is noted a small yet negative impact of LDA on the FBIAS score, as shown in the previous section (Fig. 6b). It is noticed that the sum of improved and worsened cells is not the same for all the scores as the number of undefined cells and the number of cells where the score is the same vary from score to score. The total number of grid cells, i.e. improved plus worsened plus undefined plus constant, is 2055 for all scores.

To understand the different patterns of improvement of the strokes forecast in summer and fall, it is useful to consider the maps of assimilated lightning in the two seasons (Fig. 8). In summer (Fig. 8a), most flashes occur over the land, namely the Italian mainland and the Balkans, and over the Adriatic Sea, while they shift towards the sea, especially the Tyrrhenian Sea, in fall (Fig. 8b). This shifting is a consequence of the different nature of convection in the two seasons. In summer the convection is mainly over the land because it is triggered by the solar heating in a condition of potentially unstable air. If suitable conditions are met, the solar heating destabilises the planetary boundary layer, and the potential instability is released through vigorous convection and lightning. Of course, other mechanisms can be important, as the passage of synoptic or sub-synoptic scale storms, nevertheless the mechanism discussed above is very important in summer.

In fall, the convection shifts towards the sea and develops as cooler air masses are advected over the warm Mediterranean Sea by meteorological systems. Therefore, the largest number of strokes is observed over the sea. The different distributions of the strokes in the two seasons clearly determines the impact of LDA on the strokes forecast.

3.4. Fraction skill score

The FSS results for different intensities of the strokes (1, 5, 10 strokes per WRF grid cell ($3x3km^2$)) and for different length scales are shown in Figs. 9 and 10 for summer 2020 and fall 2021, respectively. In summer,

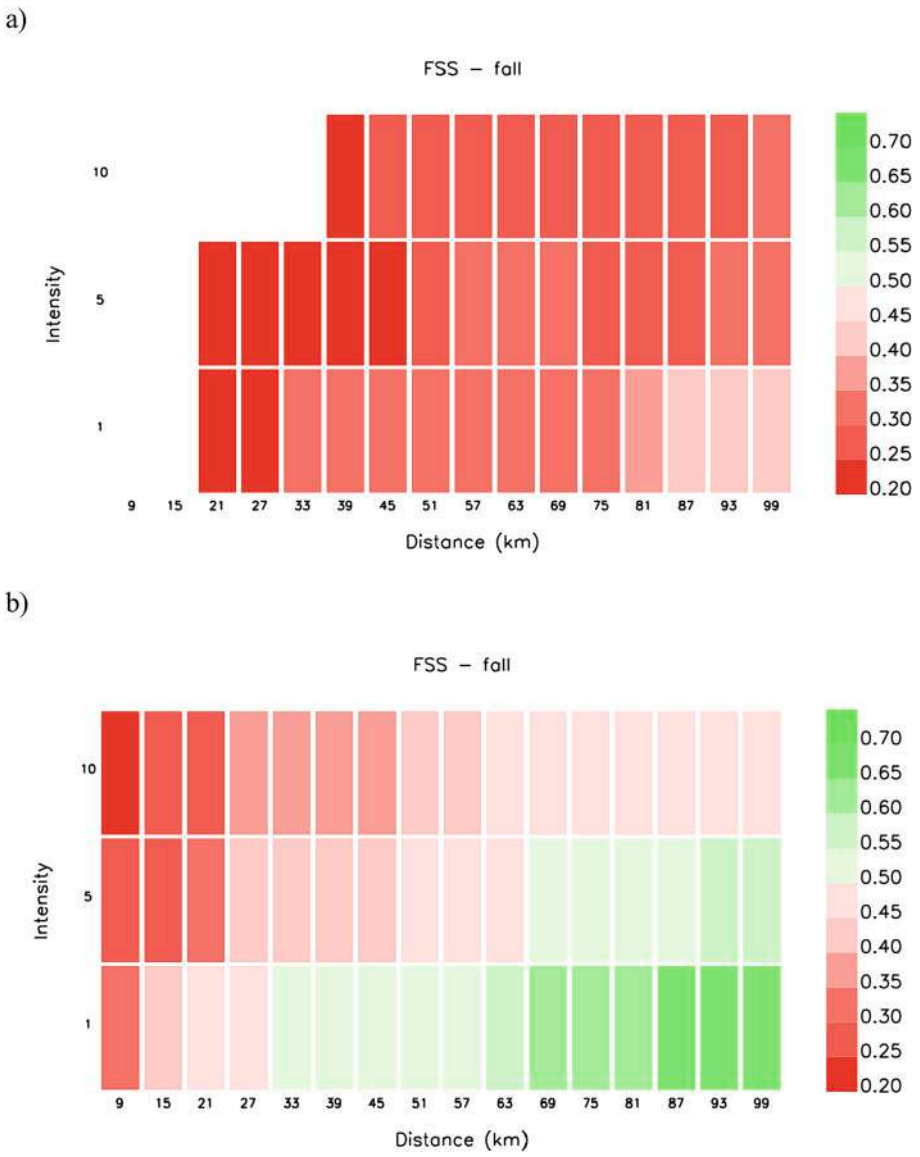

Fig. 10. As in Fig. 9 for fall 2021.

FSS of the control forecast (Fig. 9a) is lower than 0.5 for all thresholds and it increases with the length scale and for lower intensities. The FSS for the forecast with LDA (Fig. 9b) shows skillful forecasts for the three intensities. The length scales for a skillful forecast are 33, 45 and 63 km for 1, 5 and 10 strokes per WRF grid cell, respectively. The meteorological alerts for adverse weather conditions in Italy are issued by the CPD and, for this purpose, the country is divided in about 100 subareas whose typical length scale is of the order of 50 km. So, the alerts for lightning occurrence in the next 3 h are skillful and compatible with the alert areas already used by the CPD for the 1 and 5 strokes intensities.

The performance decreases in fall (Fig. 10). For simulations with LDA, a skillful forecast is attained for length scales of 33 and 69 km for the thresholds of 1 and 5 strokes per grid cell.

The results of this section show again that the strokes forecast is better in summer than in fall. There are two main reasons for this behavior: first, the number of lightning assimilated in summer is larger than in fall; second, the nature of convection in the two seasons determines a different performance of the lightning forecast. In summer there is a larger number of lightning widespread over the land, a condition that is simpler to forecast compared to more scattered and fewer strokes observed in fall.

3.5. Comparison with the previous day forecast

F22 showed that lightning forecast can be achieved with success over Italy from the previous day forecast. In their analysis they considered the strokes forecast for the whole day upscaled to a grid spacing of 24 km (as in this paper) and limited their attention to the days with at least 10,000 strokes in summer and September 2020 and to the days with at least 3000 strokes in other periods. Summer 2020 is considered also in this paper enabling a comparison with the results of F22 to answer to the following question: are we able to refine the previous day strokes forecast at the short range (0-3 h after the analysis phase) using LDA? For summer 2020, 62 simulations are already available from F22. However, to consider the whole summer, we simulated the (30) missing days as in F22. In this approach, one forecast is issued for each day: the forecast starts at 12 UTC on the day before the actual day to forecast, and initial and boundary conditions are derived from the IFS analysis/forecast cycle issued by ECMWF at the 12 UTC on the day before the actual day to forecast. The first 12 h of forecast are discarded from the analysis (spin-up time; Fig. 1b). Note that the domain, the grid resolution, the physical configuration of the WRF model, and the WRF model itself are the same as in F22, nevertheless C and F22 forecasts are similar but not the same

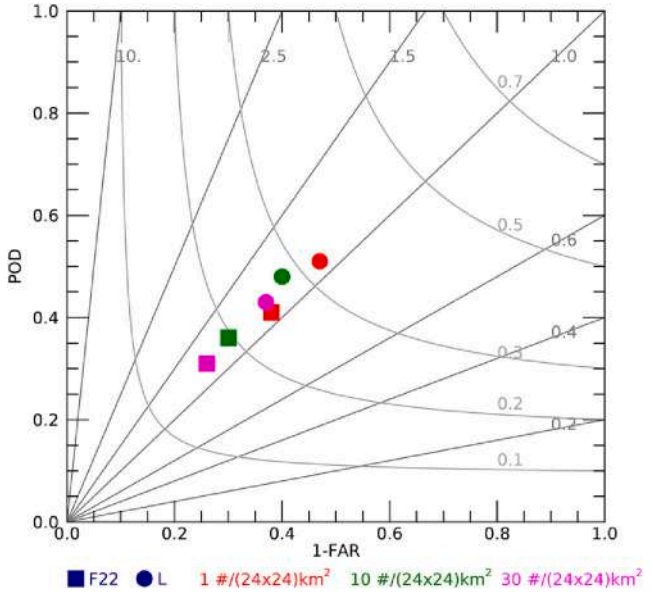

Fig. 11. Performance diagram for the first three forecast hours for the strokes prediction for the experiments L and F22. Red is for the 1 stroke/(24 km*24 km) threshold, green is for 10 stroke/(24 km*24 km), and magenta is for 30 stroke/(24 km*24 km). Straight lines represent constant values of FBIAS, while hyperbolic lines represent constant values of TS. (For interpretation of the references to colour in this figure legend, the reader is referred to the web version of this article.)

as they differ both in the simulation start time and in the spin-up time.

The comparison was done in this way: each day was divided in eight 3 h time slots and, for each of these slots, the forecast of the VSF approach with LDA (L) and that of F22 were compared. Results (Fig. 11) are discussed for the first 3 h of forecast after the ending of LDA (time slots 00–03 UTC; 06–09 UTC; 12–15 UTC; 18–21 UTC), as there is no improvement for the 3-6 h phase. The FBIAS of the F22 approach and that of this paper (L) are similar, so the frequencies of the forecasts of the strokes are similar for different thresholds. Nevertheless, the POD of the VSF approach of this paper is better than that of F22 with an improvement $>$ 10% for all thresholds. Similarly, the L forecast has a lower FAR than F22 with a reduction of about 10%. As expected, the TS score is improved by the VSF using LDA compared to the F22 forecast.

The results of this section show that the LDA improves the previous day strokes forecast at the short-range (3 h) by both increasing the correct forecasts and reducing the false alarms and the forecast with the LDA approach used in this paper should be run every 3 h to cover a full day with the best skill. This gives the opportunity to use more precise forecasts when the storm is approaching to take immediate actions to mitigate lightning related impacts.

3.6. *Analysis of the precipitation forecast*

Even if the focus of this paper is on strokes prediction, it is interesting to show the impact of the LDA on the precipitation forecast for completeness and to make the results of this paper comparable with those of previous studies. Fig. 12 shows the impact of LDA on the precipitation forecast for the first three hours of forecast in summer (panel a) and fall (panel b) through the performance diagram. Three different rainfall thresholds, namely 1 mm/3 h, 10 mm/3 h and 30 mm/3 h are considered, focusing on light, moderate and intense rainfall events.

LDA improves the performance in summer for light and moderate rainfall events (1 and 10 mm/3 h; Fig. 12a) with less, yet positive, impact for the intense rainfall event. In fall, the precipitation forecast is clearly improved for all thresholds (Fig. 12b).

The results of the resampling test for the precipitation forecast are

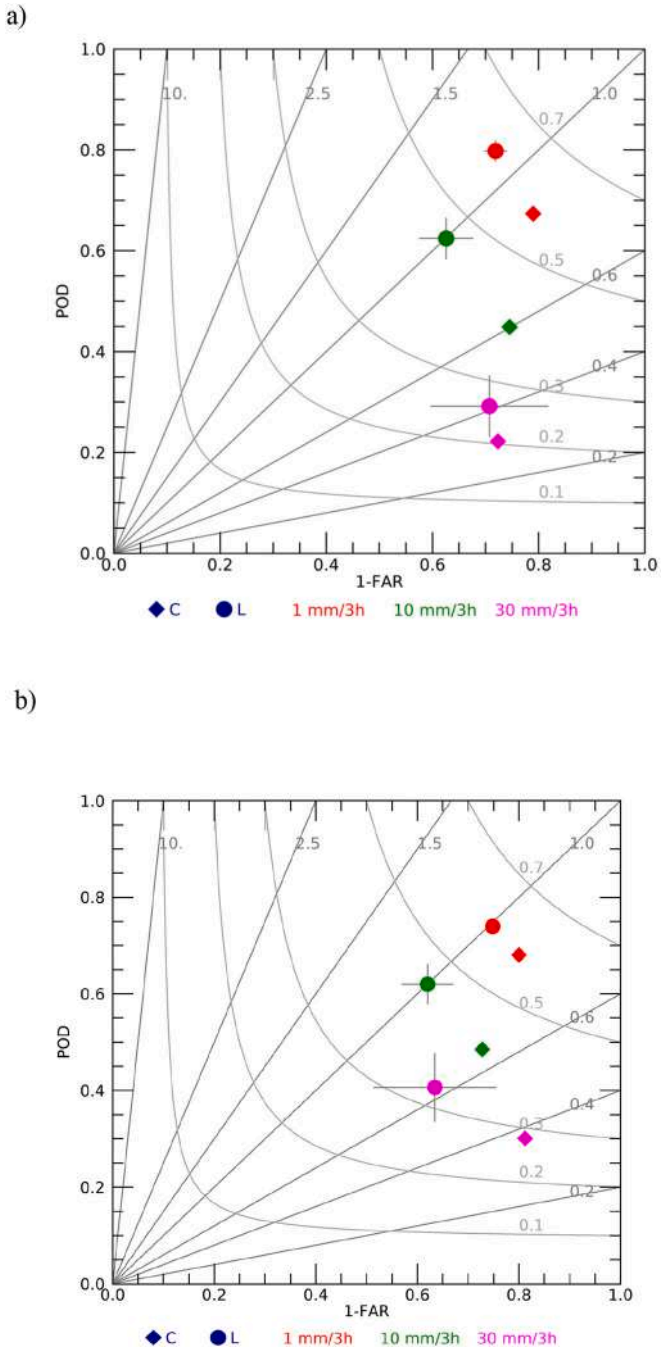

Fig. 12. a) performance diagram of the precipitation for the first three hours of forecast in summer; b) as in a) but for fall. Filled diamonds are the control forecast (C), filled circles are the forecast with LDA (L). Red symbols are for 1 mm/3 h threshold, green symbols are for 10 mm/3 h threshold, magenta symbols are for 30 mm/3 h threshold. Error bars superimposed to the L forecast, are the 5th and 95th percentile of the POD differences (between L and C) and FAR difference (between L and C) distributions computed by the resampling test.

shown in Tables 6 and 7 for summer and fall, respectively, extending the analysis to the 3-6 h forecast, to the ETS score and to new precipitation thresholds. The resampling test shows a positive impact of LDA on the rainfall forecast. In summer, the improvement is significant up to 30 mm/3 h, while in fall the positive impact of LDA goes up to heavy rainfall (50 mm/3 h). Again, we note a negligible impact of LDA on the 3-6 h forecast range. Finally, LDA increases the POD score but leads to an overestimation of rainfall, mainly for light rain in summer and for all

Table 6
Results of the resampling test for the precipitation forecast with or without LDA for summer.

	Threshold (mm/3 h)										
	1	5	10	15	20	25	30	35	40	45	50
FBIAS	99;99	99;99	99; /	99; /	99; /	99; /	99; /	/; /	/; /	/; /	/; /
ETS	/; *95*	95; /	99; /	99; /	99; /	99; /	95; /	/; /	/; /	/; /	/; /
POD	99; 99	99; 95	99; /	99; /	99; /	99; /	99; /	/; /	/; /	/; /	/; /
FAR	*99; 99*	*99*; /	*99*; /	*90*; /	/; /	/; /	/; /	/; /	/; /	/; /	/; /

The first number in each cell refers to the 0-3 h forecast; the second number refers to the 3-6 h forecast.

Table 7
As in Table 6 but for fall.

	Threshold (mm/3 h)										
	1	5	10	15	20	25	30	35	40	45	50
FBIAS	99;99	99; /	99; /	99; /	99; *99*	99; *95*	99; /	99; /	99; /	99; /	99; /
ETS	90; /	95; /	/; /	/; /	/; /	/; /	95; /	/; /	90; /	/; /	90; *90*
POD	99; /	99; /	99; /	99; /	99; *90*	99; /	99; /	95; /	99; /	/; /	99; *90*
FAR	*99;99*	*99*; *90*	*99*; /	*99*; /	*99*; /	*99*; /	*95*; /	*90*; /	/; /	*90*; /	*90*; /

thresholds in fall.

There is an interesting and apparently contradictory impact of LDA on the FAR of lightning and precipitation forecast. The LDA improves the FAR of the strokes forecast but has a detrimental impact on the FAR of the precipitation forecast. This is likely determined by the fact that LDA adds too much water vapor into the atmosphere, at least in the configuration used in this paper. This water vapor changes substantially the atmospheric behavior and convection develops rapidly into the model. As shown for the 29 August 2020 case study, between 12 and 15 UTC, the right positioning of the convection given by LDA may help to suppress spurious convection. At the same time, the water vapor added by LDA may precipitate soon after LDA or may remain into the atmosphere and, if suitable conditions are met, may precipitate later in the forecast. In any case the latter process can increase the false alarms if too much water vapor is summed by LDA.

The 29 August 2020 is a good case to discuss this issue. Fig. 13 shows the precipitation measurements, the precipitation forecast by the C experiment, and the precipitation forecast by L experiment between 12 and 15 UTC. Observations show an important precipitation event starting from Liguria and ending over northeastern Italy. Along this precipitation pattern there are several raingauges reporting >40 mm/3 h with a maximum of 90 mm/3 h. The control forecast represents only partially the observed precipitation pattern, while the forecast with LDA gives a much better representation of it. This is confirmed by the improvement of FBIAS, TS, ETS and POD scores for the 1 mm/3 h, 10 mm/3 h and 30 mm/3 h thresholds (not shown). Despite this improvement, LDA has a negative impact on the FAR forecast. Specifically, focusing of the rainfall thresholds of 1 mm/3 h, 10 mm/3 h and 30 mm/3 h the FAR of the control forecast is 0.15, 0.3 and 0.08, respectively, while the FAR of the forecast with LDA is 0.18, 0.3, 0.20, showing the increase of the FAR for the simulation with LDA. So, for the 29 August case study LDA reduces the FAR of strokes forecast but increases the FAR of the precipitation forecast. The use of explicit convection suppressing scheme (as in Erdmann et al. (2023) or Lai et al. (2019))) and the application of 3DVar could further improve the performance of LDA, but research is needed in this direction.

All in all, the results for precipitation show that LDA can substantially improve the precipitation forecast and that the impact of LDA is larger in fall compared to summer and it is confined to the first 3 h of forecast.

4. Discussion

The impact of LDA on the strokes forecast changes between summer and fall. In summer, the improvement is over the Italian mainland, over the Balkans and over the Adriatic Sea; in fall, the improvement is over the Tyrrhenian Sea and the Italian mainland. The patterns of the improvement are tied to the type of convection and to the lightning distributions in the two seasons. In summer, convection is mainly forced by the solar heating in a potentially unstable atmospheric environment and strokes occur mainly over land. In fall, the convection develops over the sea, especially the Tyrrhenian Sea, when cold air masses are advected over the warm sea by synoptic-scale meteorological systems. The improvement of the strokes forecast is mostly seen in the regions of lightning observations and LDA, i.e. over the land in summer and over the sea in fall.

The improvement of strokes forecast given by LDA is very important when considering the operational environment. The analysis of the FSS shows that the strokes forecast with LDA for 1 and 5 strokes per WRF grid cell in summer and for 1 stroke per WRF grid cell in fall are already skillful, using the alert areas defined by the CPD to issue meteorological alerts over the Italian territory. The strokes forecast without LDA is not skillful for the spatial and temporal scales considered in this paper. In addition, we showed the capability of LDA to improve the previous day lightning forecast by increasing the correct forecasts and by reducing the false alarms. This opens the possibility to take immediate actions when a storm is approaching to mitigate the impact of the lightning threat.

The impact of the LDA on the rainfall forecast is analysed shortly. As already shown in several papers over Italy, LDA can improve the very short-term precipitation forecast. The improvement is larger in fall compared to summer because of the different nature of the precipitation in the two seasons. It is noted that the LDA improves the POD of the rainfall forecast but has a negative impact on the FAR score. The FAR increase for the precipitation forecast is a limiting factor of the LDA approach used in this work. An attempt to mitigate this issue, by removing spurious convection, is given by Lynn et al. (2015), Lai et al. (2019), and by Erdmann et al. (2023). They used two different techniques to reduce the false alarms given by LDA with some success. However, further research is necessary in this direction to better quantify the impact of removing spurious convection on the precipitation forecast.

It is noticed that while lightning and precipitation are related phenomena, their forecast performance is different for the two seasons. Lightning forecast performs better in summer, while precipitation forecast is better in fall, and this is related to the different nature of the convection and precipitation in the two seasons. With respect to this point, the results of this work go in the same direction of Lynn (2017). In particular, he studied the correlation between the FSS of the precipitation and strokes' intensities for different thresholds. He found that accuracy in forecasting the probability of lightning did correspond to the

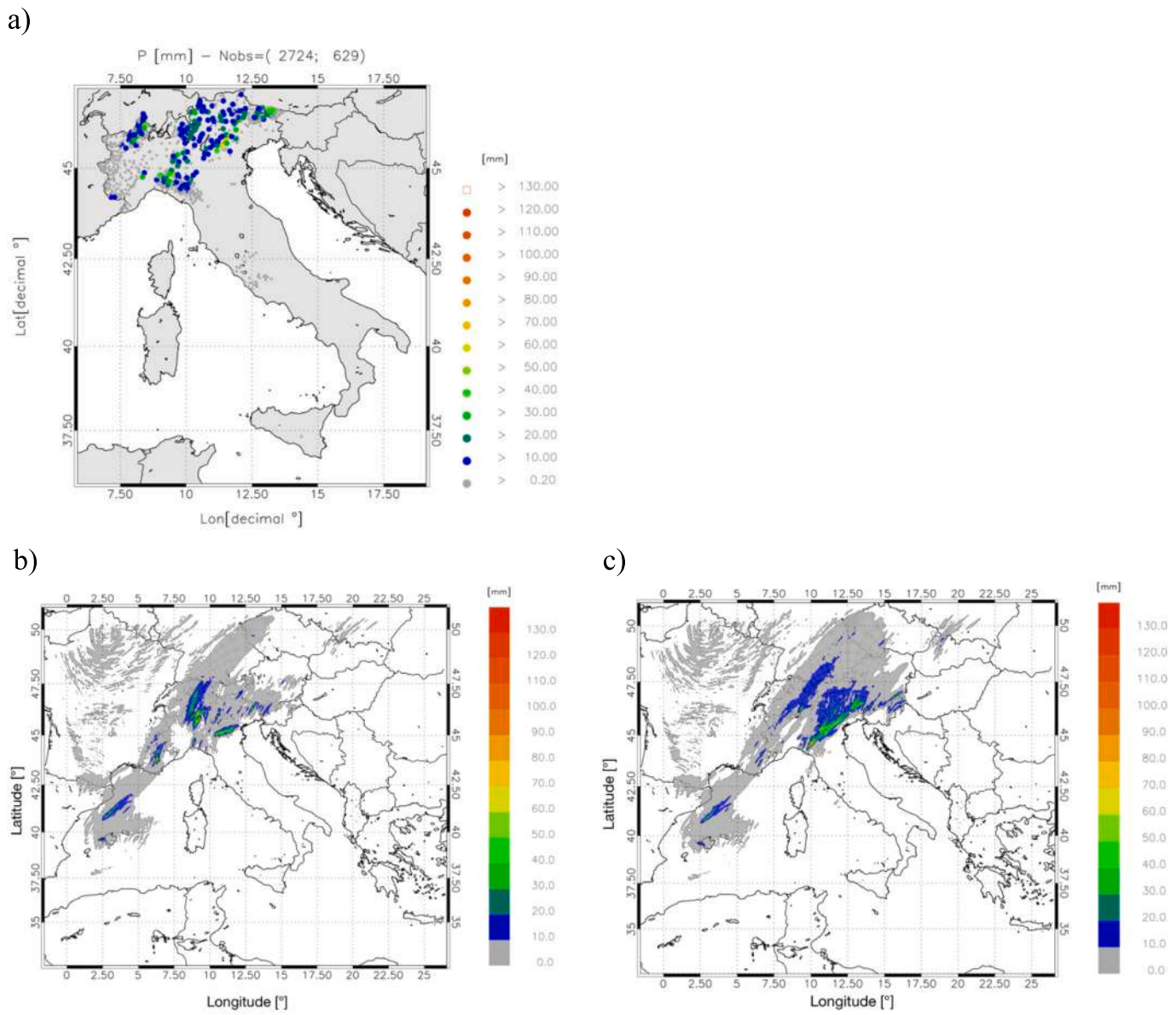

Fig. 13. a) Rainfall observed by raingauges between 12 and 15 UTC on 29 August 2020. The first number in the parenthesis in the title shows the number of raingauge observations available in the period, while the second number is the number of raingauges observing >0.2 mm; b) precipitation forecast of the control simulation between 12 and 15 UTC on 29 August 2020; c) as in b) for the simulation with LDA.

accuracy in forecasting precipitation, nevertheless the correlation coefficient decreased with increasing precipitation and strokes thresholds.

While the results of this paper highlight the good impact of LDA on the lightning forecast, the improvement is confined to the first three hours of forecast. In general, similar results are found in other papers both for lightning and precipitation forecast (Fierro et al., 2016; Lynn, 2017; Federico et al., 2019) and this is likely caused by the intrinsic unpredictability of the deep convection associated with lightning. In addition, we cannot quantify if the forecast improvement is confined in the first, second or third forecast hour as the forecasting system verified in this paper aims to predict the 3 h lightning and rainfall. However, the above cited studies show that the improvement decreases quickly with forecasting time and is larger in the first hour, compared to the second and to the third hour. There are exceptions to this behavior, as shown in Comellas Prat et al. (2021) or in Giannaros et al. (2016), who showed longer impacts of LDA on the precipitation forecast for their cases, nevertheless in these papers the statistics are shown for the whole forecast range, and it is difficult to disentangle the contribution of LDA to different forecast phases. Future studies should investigate more in detail this point using different data assimilation techniques (3DVar, Ensemble Kalman Filter) and additional observations, especially those of the METEOSAT Third Generation-Lightning Imager (MTG-LI), to improve the forecast of deep convection for longer forecast ranges.

5. Conclusions

The main findings of this paper can be summarized as follows:

- LDA improves the lightning and precipitation forecast in summer and fall. The improvement can be caused by new convection or reorganization of the convection simulated by the control forecast, without LDA;
- The positive impact of the LDA on the forecast is confined to the first three-hours;

- The pattern of improvement of the strokes forecast is different in summer and in fall and is determined by the different type of convection occurring in the two seasons;
- The forecast can be used to refine the previous days forecast when the storm is approaching;
- Lightning and rainfall, while being related phenomena, are different and the performance of their forecasts is diverse.

CRediT authorship contribution statement

Stefano Federico: Conceptualization, Methodology, Formal analysis, Visualization, Funding acquisition, Validation, Writing – original draft, Writing – review & editing. **Rosa Claudia Torcasio:** Conceptualization, Formal analysis, Methodology, Visualization, Validation, Writing – original draft, Writing – review & editing. **Jana Popova:** Funding acquisition, Methodology, Writing – original draft, Writing – review & editing. **Zbyněk Sokol:** Methodology, Writing – original draft, Writing – review & editing. **Lukáš Pop:** Methodology, Writing – original draft, Writing – review & editing. **Martina Lagasio:** Methodology, Writing – original draft, Writing – review & editing. **Barry H. Lynn:** Conceptualization, Methodology, Formal analysis, Validation, Writing – original draft, Writing – review & editing. **Silvia Puca:** Methodology, Writing – original draft, Writing – review & editing. **Stefano Dietrich:** Methodology, Writing – original draft, Writing – review & editing.

Declaration of competing interest

The authors declare that they have no known competing financial interests or personal relationships that could have appeared to influence the work reported in this paper.

Data availability

The authors can share only the WRF output on request.

Acknowledgements

This research was funded by the Mobility Plus project CNR-22–25, and the project "Improving the short-term forecast of convective events using the Meteosat Third Generation observations over Europe" Bilateral Agreement CNR/CAS 2022–2024 ID: 16962. ECMWF is acknowledged for the computing resources through the special project SPITFEDE and for providing initial and boundary conditions for the WRF model. LINET lightning network data were used through the agreement for cooperation between CNR-ISAC and Nowcast GmbH (https://www.nowcast.de/en/, accessed on 24 October 2022). Part of the work was developed inside the agreement between CPD and CNR-ISAC.

References

Alexander, G.D., Weinman, J.A., Karyampudi, V.M., Olson, W.S., Lee, A.C.L., 1999. The effect of assimilating rain rates derived from satellites and lightning on forecasts of the 1993 superstorm. Mon. Weather Rev. 127, 1433–1457. https://doi.org/10.1175/1520-0493(1999)127<1433:TEOARR>2.0.CO;2.

American Meteorological Society, 1924a. Lightning explodes dynamite. Mon. Weakly Rev. 52, 313.

American Meteorological Society, 1924b. Loss of forty-seven head of cattle by a single lightning bolt. Mon. Weakly Rev. 52, 452.

Ashley, W.S., Gilson, C.W., 2009. A reassessment of U.S. lightning mortality. Bull. Am. Meteorol. Soc. 90, 1501–1518. https://doi.org/10.1175/2009BAMS2765.1.

Barthe, C., Molinie, G., Pinty, J., 2005. Description and first results of an explicit electrical scheme in a 3D cloud resolving model. Atmos. Res. 76, 95–113. https://doi.org/10.1016/j.atmosres.2004.11.021.

Barthe, C., Deierling, W., Barth, M.C., 2010. Estimation of total lightning from various storm parameters: a cloud- resolving model study. J. Geophys. Res. 115 https://doi.org/10.1029/2010JD014405. D24202.

Betz, H.-D., Schmidt, K., Oettinger, P., Wirz, M., 2004. Lightning detection with 3D-discrimination of intracloud and cloud-to-ground discharges. J. Geophys. Res. Lett. 31 https://doi.org/10.1029/2004GL019821. L11108.

Betz, H.-D., Schmidt, K., Laroche, P., Blanchet, P., Oettinger, P., Defer, E., Dziewit, Z., Konarski, J., 2009. LINET—An international lightning detection network in Europe. Atmos. Res. 91, 564–573. https://doi.org/10.1016/j.atmosres.2008.06.012.

Chang, D.-E., Weinman, J.A., Morales, C.A., Olson, W.S., 2001. The effect of spaceborne microwave and ground-based continuous lightning measurements on forecasts of the 1998 Groundhog Day storm. Mon. Weather Rev. 129, 1809–1833. https://doi.org/10.1175/1520-0493(2001)129<1809:TEOSMA>2.0.CO;2.

Chen, Z., Qie, X., Liu, D., Xiong, Y., 2019. Lightning data assimilation with comprehensively nudging water contents at cloud-resolving scale using WRF model. Atmos. Res. 221, 72–87. https://doi.org/10.1016/j.atmosres.2019.02.001.

Comellas Prat, A., Federico, S., Torcasio, R.C., Fierro, A.O., Dietrich, S., 2021. Lightning data assimilation in the WRF-ARW model for short-term rainfall forecasts of three severe storm cases in Italy. Atmos. Res. 247, 105246 https://doi.org/10.1016/j.atmosres.2020.105246.

Dahl, J.M.L., Höller, H., Schumann, U., 2011. Modeling the flash rate of thunderstorms. Part I: Framework. Mon. Weather Rev. 139, 3093–3111. https://doi.org/10.1175/MWR-D-10-05031.1.

Defer, E., Pinty, J.-P., Coquillat, S., Martin, J.-M., Prieur, S., Soula, S., Richard, E., Rison, W., Krehbiel, P., Thomas, R., Rodeheffer, D., Vergeiner, C., Malaterre, F., Pedeboy, S., Schulz, W., Farges, T., Gallin, L.-J., Ortéga, P., Ribaud, J.-F., Anderson, G., Betz, H.-D., Meneux, B., Kotroni, V., Lagouvardos, K., Roos, S., Ducrocq, V., Roussot, O., Labatut, L., Molinié, G., 2015. An overview of the lightning and atmospheric electricity observations collected in southern France during the HYdrological cycle in Mediterranean EXperiment (HyMeX), Special Observation Period 1. Atmos. Meas. Tech. 8, 649–669. https://doi.org/10.5194/amt-8-649-2015.

Ducrocq, V., Braud, I., Davolio, S., Ferretti, R., Flamant, C., Jansa, A., Kalthoff, N., Richard, E., Taupier-Letage, I., Ayral, P.-A., Belamari, S., Berne, A., Borga, M., Boudevillain, B., Bock, O., Boichard, J.-L., Bouin, M.-N., Bousquet, O., Bouvier, C., Chiggiato, J., Cimini, D., Corsmeier, U., Coppola, L., Cocquerez, P., Defer, E., Delanoë, J., Di Girolamo, P., Doerenbecher, A., Drobinski, P., Dufournet, Y., Fourrié, N., Gourley, J.J., Labatut, L., Lambert, D., Le Coz, J., Marzano, F.S., Molinié, G., Montani, A., Nord, G., Nuret, M., Ramage, K., Rison, W., Roussot, O., Said, F., Schwarzenboeck, A., Testor, P., Van Baelen, J., Vincendon, B., Aran, M., Tamayo, J., 2014. HyMeX-SOP11: the field campaign dedicated to heavy precipitation and flash flooding in the Northwestern Mediterranean. B. Am. Meteorol. Soc. 95, 1083–1100. https://doi.org/10.1175/BAMS-D-12-00244.1.

Dudhia, J., 1989. Numerical study of convection observed during the Winter Monsoon Experiment using a mesoscale two- dimensional model. J. Atmos. Sci. 46, 3077–3107. https://doi.org/10.1175/1520- 0469(1989)046<3077:NSOCOD>2.0.CO;2.

Erdmann, F., Defer, E., Caumont, O., Blakeslee, R.J., Pédeboy, S., Coquillat, S., 2020. Concurrent satellite and ground-based lightning observations from the Optical Lightning Imaging Sensor (ISS-LIS), the low-frequency network Meteorage and the SAETTA Lightning Mapping Array (LMA) in the northwestern Mediterranean region. Atmos. Meas. Tech. 13, 853–875. https://doi.org/10.5194/amt-13-853-2020.

Erdmann, F., Caumont, O., Defer, E., 2023. Assimilation of Meteosat Third Generation (MTG) Lightning Imager (LI) pseudo-observations in AROME-France – proof of concept. Nat. Hazards Earth Syst. Sci. 23, 2821–2840. https://doi.org/10.5194/nhess-23-2821-2023.

Federico, S., Avolio, E., Petracca, M., Panegrossi, G., Sanò, P., Casella, D., Dietrich, S., 2014. Simulating lightning into the RAMS model: Implementation and preliminary results. Nat. Hazards Earth Syst. Sci. 14, 2933–2950. https://doi.org/10.5194/nhess-14-2933-2014.

Federico, S., Petracca, M., Panegrossi, G., Dietrich, S., 2017. Improvement of RAMS precipitation forecast at the short- range through lightning data assimilation. Nat. Hazards Earth Syst. Sci. 17, 61–76. https://doi.org/10.5194/nhess-17-61-2017.

Federico, S., Torcasio, R.C., Avolio, E., Caumont, O., Montopoli, M., Baldini, L., Vulpiani, G., Dietrich, S., 2019. The impact of lightning and radar reflectivity factor data assimilation on the very short-term rainfall forecasts of RAMS@ISAC: Application to two case studies in Italy. Nat. Hazards Earth Syst. Sci. 19, 1839–1864. https://doi.org/10.5194/nhess-19-1839-2019.

Federico, S., Torcasio, R.C., Puca, S., Vulpiani, G., Comellas Prat, A., Dietrich, S., Avolio, E., 2021. Impact of radar reflectivity and lightning data assimilation on the rainfall forecast and predictability of a summer convective thunderstorm in Southern Italy. Atmosphere 12, 958. https://doi.org/10.3390/atmos12080958.

Federico, S., Torcasio, R.C., Lagasio, M., Lynn, B.H., Puca, S., Dietrich, S., 2022. A year-long total lightning forecast over Italy with a dynamic lightning scheme and WRF. Remote Sens. 14 3244. https://doi.org/10.3390/rs14143244.

Fierro, A.O., Mansell, E.R., Ziegler, C.L., MacGorman, D.R., 2012. Application of a lightning data assimilation technique in the WRF-ARW Model at cloud-resolving scales for the tornado outbreak of 24 May 2011. Mon. Weakly Rev. 140, 2609–2627. https://doi.org/10.1175/MWR-D-11-00299.1.

Fierro, A.O., Mansell, E.R., MacGorman, D.R., Ziegler, C.L., 2013. The implementation of an explicit charging and discharge lightning scheme within the WRF-ARW Model: benchmark simulations of a continental squall line, a tropical cyclone, and a winter storm. Mon. Weakly Rev. 141, 2390–2415. https://doi.org/10.1175/MWR-D-12-00278.1.

Fierro, A., Gao, J., Ziegler, C.L., Mansell, E.R., MacGorman, D.R., Dembek, S.R., 2014. Evaluation of a cloud-scale lightning data assimilation technique and a 3DVAR method for the analysis and short-term forecast of the 29 June 2012 Derecho event. Mon. Weather Rev. 142, 183–202. https://doi.org/10.1175/MWR-D-13-00142.1.

Fierro, A.O., Gao, J., Ziegler, C.L., Calhoun, K.M., Mansell, E.R., MacGorman, D.R., 2016. Assimilation of flash extent data in the variational framework at convection-allowing scales: proof-of-concept and evaluation for the short-term forecast of the 24 May 2011 Tornado outbreak. Mon. Weather Rev. 144, 4373–4393. https://doi.org/10.1175/MWR-D-16-0053.1.

Giannaros, T.M., Kotroni, V., Lagouvardos, K., 2016. WRF-LTNGDA: a lightning data assimilation technique implemented in the WRF model for improving precipitation forecasts. Environ. Model Softw. 76, 54–68.
Hamill, T.M., 1999. Hypothesis tests for evaluating numerical precipitation forecasts. Weather Forecast. 14, 155–167. https://doi.org/10.1175/1520-0434(1999)0142.0.CO;2.
Hodanish, S., Holle, R., Lindsey, D.T., 2004. A small updraft producing a fatal lightning flash. Weather Forecast. 19, 627–632. https://doi.org/10.1175/1520-0434(2004)019<0627:ASUPAF>2.0.CO;2.
Holle, R.L., López, R.E., Arnold, L.J., Endres, J., 1996. Insured lightning-caused property damage in three western states. J. Appl. Meteorol. 35, 1344–1351. https://doi.org/10.1175/1520-0450(1996)035<1344:ILCPDI>2.0.CO;2.
Holle, R.L., López, R.E., Navarro, B.C., 2005. Deaths, injuries, and damages from lightning in the United States in the 1890s in comparison with the 1990s. J. Appl. Meteorol. 44, 1563–1573. https://doi.org/10.1175/JAM2287.1.
Holle, R.L., Said, R.K., Brooks, W.A., 2018. Monthly GLD360 lightning percentages by continent. In: Proceedings of the 7th International Lightning Meteorology Conference, Fort Lauderdale, FL, USA,v12–15 March 2018.
Höller, H., Betz, H.-D., 2010. Study on Inter-Comparison of LIS and Ground-Based Lightning Location System Observations, Report ITT No. 09/996, EUMETSAT, Deutsches Zentrum für Luft- und Raumfahrt. https://doi.org/10.5194/amt-13-2965-2020.
Janjic, Z.I., 1994. The step-mountain eta coordinate model: further developments of the convection, viscous sublayer, and turbulence closure schemes. Mon. Weather Rev. 122, 927–945. https://doi.org/10.1175/1520-0493(1994)122<0927:TSMECM>2.0.CO;2.
Jones, C.D., MacPherson, B., 1997. A latent heat nudging scheme for the assimilation of precipitation data into an operational mesoscale model. Meteorol. Appl. 4, 269–277. https://doi.org/10.1017/S1350482797000522.
Kain, J.S., Fritsch, J.M., 1990. A one-dimensionalentraining/detraining plume model and its application in convective parameterization. J. Atmos. Sci. 47, 2784–2802. https://doi.org/10.1175/1520-0469(1990)047<2784:AODEPM>2.0.CO;2.
Koshak, W.J., Cummins, K.L., Buechler, D.E., Vant-Hull, B., Blakeslee, R.J., Williams, E. R., Peterson, H.S., 2015. Variability of CONUS lightning in 2003–2012 and associated impacts. J. Appl. Meteorol. Climatol. 54, 15–41. https://doi.org/10.1175/JAMC-D-14-0072.1.
Lagasio, M., Parodi, A., Procopio, R., Rachidi, F., Fiori, E., 2017. Lightning potential Index performances in multimicrophysical cloud-resolving simulations of a back-building mesoscale convective system: the Genoa 2014 event. J. Geophys. Res. 122, 4238–4257. https://doi.org/10.1002/2016JD026115.
Lagouvardos, K., Kotroni, V., Betz, H.-D., Schmidt, K., 2009. A comparison of lightning data provided by ZEUS and LINET networks over Western Europe. Nat. Hazards Earth Syst. Sci. 9, 1713–1717. https://doi.org/10.5194/nhess-9-1713-2009.
Lai, A., Gao, J., Koch, S.E., Wang, Y., Pan, S., Fierro, A.O., Cui, C., Min, J., 2019. Assimilation of radar radial velocity, reflectivity, and pseudo–water vapor for convective-scale NWP in a variational framework. Mon. Weather Rev. 147, 2877–2900. https://doi.org/10.1175/MWR-D-18-0403.1.
Lopez, R.E., Heitkamp, T.A., 1995. Lightning casualties and property damage in Colorado from 1950 to 1991 based on storm Data. Weather Forecast. 10, 114–126. https://doi.org/10.1175/1520-0434(1995)010<0114:LCAPDI>2.0.CO;2.
Lopez, R.E., Holle, R.L., 1996. Fluctuations of lightning casualties in the United States: 1959–1990. J. Clim. 9, 608–615.
Lynn, B.H., 2017. The usefulness and economic value of total lightning forecasts made with a dynamic lightning scheme coupled with lightning data assimilation. Weather Forecast. 32, 645–663. https://doi.org/10.1175/WAF-D-16-0031.1.
Lynn, B.H., Yair, Y., 2010. Prediction of lightning flash density with the WRF model. Adv. Geosci. 23, 11–16. https://doi.org/10.5194/adgeo-23-11-2010.
Lynn, B.H., Yair, Y., Price, C., Kelman, G., Clark, A.J., 2012. Predicting cloud-to-ground and intracloud lightning in weather forecast models. Weather Forecast. 27, 1470–1488. https://doi.org/10.1175/WAF-D-11-00144.1.
Lynn, B.H., Kelman, G., Ellrod, G., 2015. An evaluation of the efficacy of using observed lightning to improve convective lightning forecasts. Weather Forecast. 30, 405–423. https://doi.org/10.1175/WAF-D-13-00028.1.
Lynn, B.H., Cohen, S., Druyan, L., Phillips, A.S., Shea, D., Krugliak, H., Khain, A.P., 2020. An examination of the impact of grid spacing on WRF simulations of wintertime precipitation in the Mid-Atlantic United States. Weather Forecast. 35, 2317–2343. https://doi.org/10.1175/WAF-D-19-0154.1.
MacGorman, D., Straka, J., Ziegler, C., 2001. A lightning parameterization for numerical cloud models. J. Appl. Meteorol. 40, 459–478. https://doi.org/10.1175/1520-0450(2001)040<0459:ALPFNC>2.0.CO;2.
Mansell, E.R., MacGorman, D.R., Ziegler, C.L., Straka, J.M., 2002. Simulated three-dimensional branched lighting in a numerical thunderstorm model. J. Geophys. Res. 107, 4075. https://doi.org/10.1029/2000JD000244.
Mansell, E.R., MacGorman, D., Ziegler, C., Straka, J.M., 2005. Charge structure and lightning sensitivity in a simulated multicell thunderstorm. J. Geophys. Res. 110 https://doi.org/10.1029/2004JD005287. D12101.
Mansell, E.R., Ziegler, C.L., MacGorman, D.R., 2007. A lightning data assimilation technique for mesoscale forecast models. Mon. Weather Rev. 135, 1732–1748.
McCaul Jr., E.W., Priftis, G., Case, J.L., Chronis, T., Gatlin, P.N., Goodman, S.J., Kong, F., 2020. Sensitivities of the WRF lightning forecasting algorithm to parameterized microphysics and boundary layer schemes. Weather Forecast. 35, 1545–1560. https://doi.org/10.1175/WAF-D-19-0101.1.
McCaul, E.W., Goodman, S.J., LaCasse, K.M., Cecil, D.J., 2009. Forecasting lightning threat using cloud-resolving model simulations. Weather Forecast. 24, 709–729. https://doi.org/10.1175/2008WAF2222152.1.
Mittermaier, M., Wilkinson, J., Csima, G., Goodman, S., Virts, K., 2022. Convective-scale numerical weather prediction and warnings over Lake Victoria: Part I – Evaluating a lightning diagnostic. Meteorol. Appl. 29, e2038 https://doi.org/10.1002/met.2038.
Mlawer, E.J., Taubman, S.J., Brown, P.D., Iacono, M.J., Clough, S.A., 1997. Radiative transfer for inhomogeneous atmospheres: RRTM, a validated correlated-k model for the longwave. J. Geophys. Res. Space 102, 16663–16682. https://doi.org/10.1029/97JD00237.
Papadopoulos, A., Chronis, T.G., Anagnostou, E.N., 2005. Improving convective precipitation forecasting through assimilation of regional lightning measurements in a mesoscale model. Mon. Weather Rev. 133, 1961–1977. https://doi.org/10.1175/MWR2957.1.
Pessi, A.T., Businger, S., 2009. Relationships among lightning, precipitation, and hydrometeor characteristics over the North Pacific Ocean. J. Appl. Meteorol. Climatol. 48, 833–848. https://doi.org/10.1175/2008JAMC1817.1.
Peterson, T.C., Easterling, D.R., Karl, T.R., Groisman, P., Nicholls, N., Plummer, N., Torok, S., Auer, I., Boehm, R., Gullett, D., Vincent, L., Heino, R., Tuomenvirta, H., Mestre, O., Szentimrey, T., Salinger, J., Forland, E.J., Hanssen-Bauer, I., Alexandersson, H., Jones, P., Parker, D., 1998. Homogeneity adjustments of in situ atmospheric climate data: a review. Int. J. Climatol. 18, 1493–1517. https://doi.org/10.1002/(SICI)1097-0088(19981115)18:13<1493::AID-JOC329>3.0.CO;2-T.
Petracca, M., 2016. Studio dell'Attività Elettrica Nelle Nubi Temporalesche ed Utilizzo dei Dati di Fulminazione per la Meteorologia Operativa. Ph.D. Thesis,. University of Ferrara, Ferrara, Italy, p. 231p.
Popová, J., Sokol, Z., Šlegl, J., Wang, P., Chou, Y.-L., 2022. Research cloud electrification model in the Wisconsin dynamic/microphysical model 2: charge structure in an idealized thunderstorm and its dependence on ion generation rate. Atmos. Res. 270, 106090 https://doi.org/10.1016/j.atmosres.2022.106090.
Popová, J., Sokol, Z., Wang, P., Svoboda, J., 2023. Observations and modelling of the winter thunderstorm on 4 February 2022 at the Milešovka meteorological observatory. Quart. J. Royal Meteorol. Soc. https://doi.org/10.1002/qj.4572 (n.d).
Price, C., Rind, D., 1992. A simple lightning parameterization for calculating global lightning distributions. J. Geophys. Res. 97, 9919–9933. https://doi.org/10.1029/92JD00719.
Qie, X., Zhu, R., Yuan, T., Wu, X., Li, W., Liu, D., 2014. Application of total-lightning data assimilation in a mesoscale convective system based on the WRF model. Atmos. Res. 145–146, 255–266. https://doi.org/10.1016/j.atmosres.2014.04.012.
Roberts, N.M., Lean, H.W., 2008. Scale-selective verification of rainfall accumulations from high-resolution forecasts of convective events. Mon. Weather Rev. 136, 78–97. https://doi.org/10.1175/2007MWR2123.1.
Roebber, P.J., 2009. Visualizing multiple measures of forecast quality. Weather Forecast. 24, 601–608. https://doi.org/10.1175/2008WAF2222159.1.
Romps, D.M., Charn, A.B., Holzworth, R.H., Lawrence, W.E., Molinari, J., Vollaro, D., 2018. CAPE times P explains lightning over land but not the land-ocean contrast. Geophys. Res. Lett. 45, 12623–12630. https://doi.org/10.1029/2018GL080267.
Rorig, M.L., Ferguson, S.A., 2002. The 2000 fire season: Lightning-caused fires. J. Appl. Meteorol. 41, 786–791. https://doi.org/10.1175/1520-0450(2002)041<0786:TFSLCF>2.0.CO;2.
Schultz, C.J., Petersen, W.A., Carey, L.D., 2009. Preliminary development and evaluation of lightning jump algorithms for the real-time detection of severe weather. J. Appl. Meteorol. Climatol. 48, 2543–2563. https://doi.org/10.1175/2009JAMC2237.1.
Skamarock, W.C., Klemp, J.B., Dudhia, J., Gill, D.O., Liu, Z., Berner, J., Wang, W., Powers, J.G., Duda, M.G., Barker, D.M., Huang, X.-Y., 2019. A Description of the Advanced Research WRF Version 4; No. NCAR/TN-556+STR, NCAR Technical Note. National Center for Atmospheric Research, Boulder, CO, USA. https://doi.org/10.5065/1dfh-6p97, 145p.
Solomon, R., Baker, M., 1996. A one-dimensional lightning parameterization. J. Geophys. Res. 101, 14983–14990.
Solomon, R., Medaglia, C.M., Adamo, C., Dietrich, S., Mugnai, A., Biader Ceipidor, U., 2005. An explicit microphysics thunderstorm model. Int. J. Model. Simul. 25, 112–118. https://doi.org/10.1080/02286203.2005.11442325.
Thompson, G., Field, P.R., Rasmussen, R.M., Hall, W.D., 2008. Explicit forecasts of winter precipitation using an improved bulk microphysics scheme. Part II: implementation of a new snow parameterization. Mon. Weather Rev. 136, 5095–5115. https://doi.org/10.1175/2008MWR2387.1.
Torcasio, R.C., Federico, S., Comellas Prat, A., Panegrossi, G., D'Adderio, L.P., Dietrich, S., 2021. Impact of lightning data assimilation on the short-term precipitation forecast over the Central Mediterranean Sea. Remote Sens. 13, 682. https://doi.org/10.3390/rs13040682.
Torcasio, R.C., Papa, M., Del Frate, F., Dietrich, S., Toffah, F.E., Federico, S., 2023. Study of the intense meteorological event occurred in september 2022 over the marche region with WRF model: impact of lightning data assimilation on rainfall and lightning prediction. Atmosphere 14, 1152. https://doi.org/10.3390/atmos14071152.
Wallmann, J., Milne, R., Smallcomb, C., Mehle, M., 2010. Using the 21 June 2008 California lightning outbreak to improve dry lightning forecast procedures. Weather Forecast. 25 https://doi.org/10.1175/2010WAF2222393.1, 14471462.
Williams, E.R., 1989. The tripole structure of thunderstorms. J. Geophys. Res. 94, 13151–13167. https://doi.org/10.1029/JD094iD11p13151.
Williams, E., Renno, N., 1993. An analysis of the conditional instability of the tropical atmosphere. Mon. Weather Rev. 121, 21–36. https://doi.org/10.1175/1520-0493(1993)121<0021:AAOTCI>2.0.CO;2.

Wong, J., Barth, M.C., Noone, D., 2013. Evaluating a lightning parameterization based on cloud-top height for mesoscale numerical model simulations. Geosci. Model Dev. 6, 429–443. https://doi.org/10.5194/gmd-6-429-2013.

Yair, Y., Lynn, B.H., Price, C., Kotroni, V., Lagouvardos, K., Morin, E., Mugnai, A., Llasat, M.C., 2010. Predicting the potential for lightning activity in Mediterranean storms based on the Weather Research and forecasting (WRF) model dynamic and microphysical fields. J. Geophys. Res. 115 https://doi.org/10.1029/2008JD010868. D04205.

Yoshida, S., Morimoto, T., Ushio, T., Kawasaki, Z., 2009. A fifth-power relationship for lightning activity from Tropical Rainfall measuring Mission satellite observations. J. Geophys. Res. 114 https://doi.org/10.1029/2008JD010370. D09104.